

FINAL TECHNICAL REPORT

USGS Award No. 08HQGR0096

UTILITY OF COMBINED AERIAL PHOTOGRAPHY AND DIGITAL IMAGERY FOR FAULT TRACE MAPPING IN DIVERSE TERRAIN AND VEGETATION REGIMES

Jerome A. Treiman
Co-Principal Investigator
California Geological Survey
888 S. Figueroa St., Ste. 475
Los Angeles CA 90017
Tel: 213-239-0889
Fax: 213-239-0894
Email: jtreiman@constrv.ca.gov

Florante G. Perez
Co-Principal Investigator
California Geological Survey
801 K. St., MS 12-32
Sacramento CA 95814
Tel: 916-322-0203
Fax: 916-322-4765
Email: aperez@constrv.ca.gov

William A. Bryant
Co- Investigator
California Geological Survey
801 K. St., MS 12-32
Sacramento CA 95814
Tel: 916-323-9672
Fax: 916-445-3334
Email: bbryant@constrv.ca.gov



April 20, 2010



Research supported by the U.S. Geological Survey (USGS), Department of the Interior, under USGS award number 08HQGR0096. The views and conclusions contained in this document are those of the authors and should not be interpreted as necessarily representing the official policies, either expressed or implied, of the U.S. Government.

Utility of Combined Aerial Photography and Digital Imagery for Fault Trace Mapping in Diverse Terrain and Vegetation Regimes

Jerome Treiman, Florante Perez, William Bryant

Abstract

Various types of aerial imagery have long been recognized for their value in fault trace mapping. Most recently, the value of LiDAR imagery to “see through” vegetation has been recognized for forested areas. In this study we compared the effectiveness of shaded relief imagery derived from high-resolution LiDAR digital elevation models to standard aerial photography and to digital multi-spectral imagery for identifying and mapping active faults in moderate to sparsely vegetated terrain in southern California. The digital imagery included recently acquired digital stereo imagery. We also compared LiDAR-derived imagery to several combinations of draped or fused digital imagery. Additionally, we looked at the use of accurately georeferenced digital imagery for the accurate registration of interpreted data from older non-registered aerial photography. The study areas spanned varying terrain and geology.

We found that no single type of imagery could serve as a stand-alone product for fault interpretation, as most image types added some value not found in other imagery. However, stereo imagery (photographic or digital) proved the most useful in the areas evaluated in this study. The lack of tonal distinctions in the LiDAR imagery was a detriment in areas where geomorphic expression was absent, although combination with spectral imagery compensated for this to some small degree. Georeferenced digital imagery worked very well for improving the locational accuracy of many features interpreted from older aerial imagery. Several observations in this study demonstrated the continued need for ground-truthing the remote sensing observations and interpretations.

Table of Contents

A. Purpose	1
B. Approach	1
C. Original Mapping	4
D. Setting	7
E. Remote Sensing Imagery	8
Imagery Acquisition.....	8
Imagery Preparation and Processing.....	10
Processed/Derived Imagery.....	11
Imagery Visualization and Analysis.....	13
F. Results.....	17
For the Indio area.....	17
For the Yucaipa area.....	25
G. Analysis and Discussion	31
General comments on utility of the processed/derived imagery.....	31
Caveats or Limitations.....	39
Accuracy and Precision.....	40
H. Conclusions.....	42
I. Resultant Publications	43
J. Further Work	43
K. Acknowledgements	43
L. References.....	43
M. Appendices	44

List of Figures

Figure 1.	Index map of San Andreas fault and two study areas in southern California	2
Figure 2a.	Indio study area showing previously mapped fault traces.....	5
Figure 2b.	Yucaipa study area showing previously mapped fault traces.....	6
Figure 3a.	Graphic displays of some of the processed/derived imagery used in the fault interpretation for the Indio study area	14
Figure 3b.	Graphic displays of some of the processed/derived imagery used in the fault interpretation for the Yucaipa study area	15
Figure 4.	Examples of features mappable in different imagery and combinations	18
Figure 5a.	Consolidated plot of fault-related geomorphic features interpreted in the Indio study area (NW Half and SE Half)	19-20
Figure 5b.	Consolidated plot of fault-related geomorphic features interpreted in the Yucaipa study area.....	21
Figure 6a.	Interpreted fault traces in the Indio area	22
Figure 6b.	Interpreted fault traces in the Yucaipa area	26
Figures 7a-b.	Examples of LiDAR artifacts	36-37
Figures 8a-b.	Improved locational accuracy of interpreted features in vintage aerial photographs with the help of LiDAR.....	41

List of Tables

Table 1.	Summary of properties and characteristics of the acquired Imagery	9
Table 2.	Summary of the various image processing techniques used to generate the processed/derived imagery	12
Table 3a.	Fault-related geomorphic features mapped in the Indio study area.....	Appendix
Table 3b.	Fault-related geomorphic features mapped in the Yucaipa study area.....	Appendix
Table 4a.	Interpreted faults in the Indio study area showing the proportion of fault traces identified in each imagery type	23
Tables 4b-d.	Interpreted faults in the Yucaipa study area showing the proportion of fault traces identified in each imagery type	27
Tables 5a-d	Imagery types with rankings of value for mapping each fault trace	32-35

A. Purpose

This study is intended to compare the utility of various aerial imagery types in the identification of active surface faults. We have done comparative mapping of recently active surface traces of the San Andreas Fault in southern California using conventional aerial photography, LiDAR digital elevation models (Airborne Laser Swath Mapping from the B4 campaign), recently acquired ADS40 imagery (Stereo, NAIP & ISTAR) and multi-spectral imagery (ASTER).

Current methods of fault interpretation from aerial imagery, individually, have certain strengths and weaknesses. Vintage (pre-development) aerial photos provide stereo viewing and show the landform prior to human modification, but commonly lack color and have limitations in accuracy of location due to lack of georeferencing and the inherent distortions in the medium. LiDAR terrain data have high spatial resolution and accuracy that can reveal subtle geomorphic features, can be viewed as detailed shaded-relief images illuminated from any direction and have the capability of virtually removing vegetation, but the imagery is limited to the modern landscape, does not easily differentiate vegetation and cultural features from geologic features and is relatively costly to acquire for new (not previously flown) areas. High resolution digital stereo imagery can often differentiate lithology, soil moisture content and vegetation that can be useful for mapping the surface trace of active faults; however, like aerial photos, the ground surface can also be obscured by vegetation. Multi-spectral imagery from several sources at varying resolutions makes advantageous use of single and multiple wavelengths of the electromagnetic spectrum but is also limited to the current landscape and requires considerable processing.

The value of Airborne Laser Swath Mapping (ALSM) in areas with a tall, obscuring vegetation canopy has already been well demonstrated (e.g. Prentice and others, 2004; Whitehill, Prentice and Mynatt, 2009). We are evaluating the relative value of LIDAR data in somewhat less densely vegetated terrain as compared with several other types of terrain data (photographic and digital).

One objective is to use the geographic precision of the digital imagery, especially LiDAR, to accurately locate fault traces interpreted from vintage aerial photography and other imagery. A second objective is to merge the LiDAR DEM with multi-spectral imagery, adding detailed topographic information to the unique surface information contained in spectral reflectance and emittance. By using several different types of imagery we will be able to judge which are more suitable for various field conditions.

B. Approach

Two test areas were selected for this study that provide contrasting terrain and vegetation conditions. These two areas, shown on Figure 1, are along the San Andreas Fault near the cities of Indio and Yucaipa in southern California. The Indio area has very little vegetation so that the surface morphology and character are visible in most image types. Strands of the fault lie partly along the abrupt southwest front of the Indio Hills and then project southward beyond the hill front into more subdued desert terrain. Some of this area has been significantly modified by human activity. Geologic variation

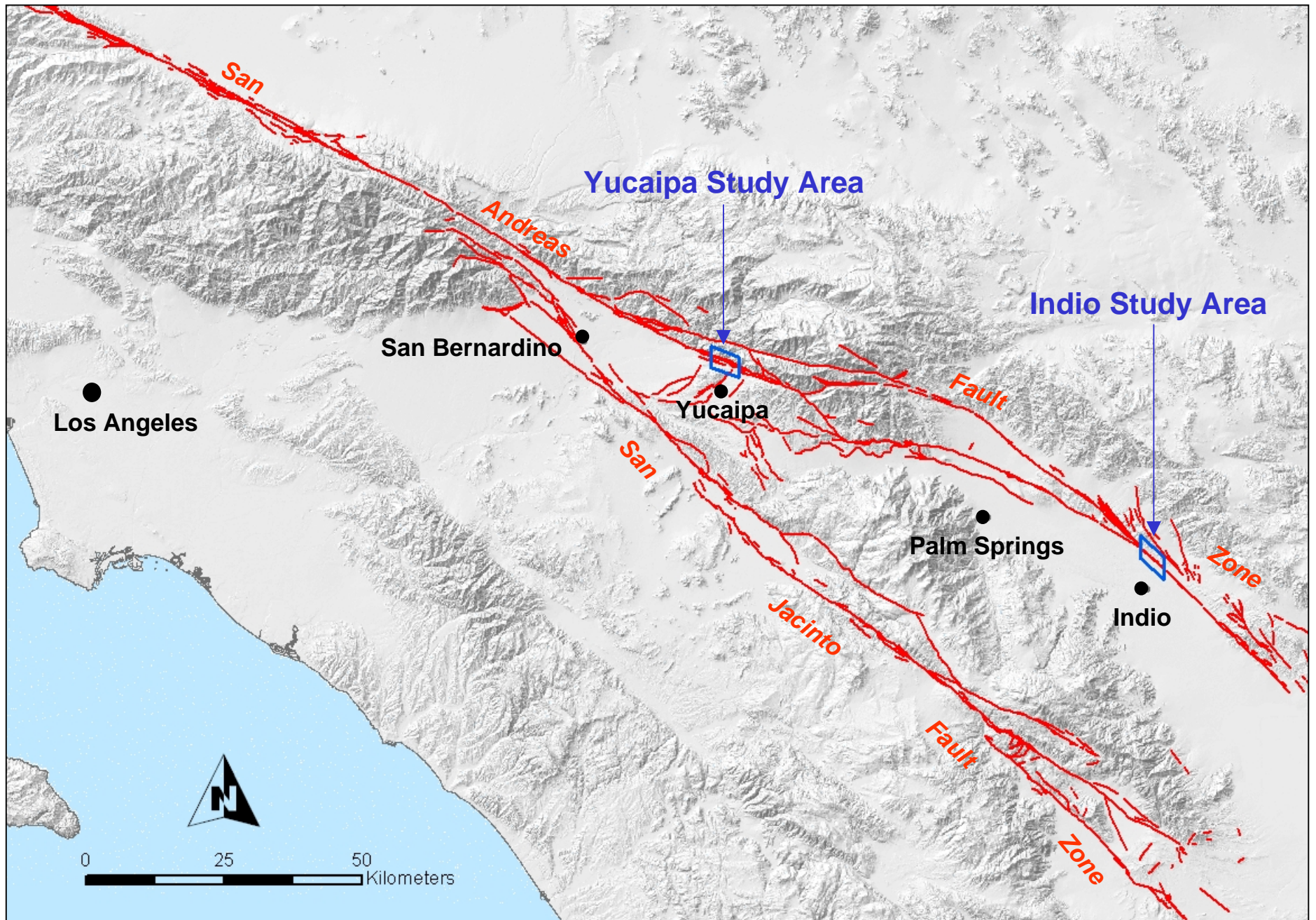


Figure 1. Index map of San Andreas fault and two study areas in southern California.

within the area is limited, with the main contrast corresponding to the topographic front. The Yucaipa area differs from the Indio area in several aspects, most evident of which is the amount of vegetation growing on the slopes and associated thicker soil, which mask many of the finer fault features. Also, the faults in the Yucaipa area lie largely within uplifted terrain with greater local relief than the Indio area. The underlying earth materials vary considerably, from bedrock to landslide to alluvium.

Several types of imagery were acquired and interpreted. These included standard black and white aerial photography, modern digital color imagery, and ALSM/LiDAR DEM (Table 1). Stereo viewing of the study areas was possible with standard aerial photography as well as with ADS40 Stereo imagery. A three-dimensional (3D) view was effected with the LiDAR DEM (shaded relief) imagery. Each image type, alone and in selected combinations, was independently interpreted by a geologist for lineaments and other geomorphic features that could be associated with faulting. Interpretation was performed at a variety of scales to detect both large and small-scale features.

The interpreted features were compiled first on separate map layers and then a composite map was prepared, consolidating features that were evidently the same to a best-fit location. Vintage aerial photo interpretation was separately compiled. The composite map was used along with the vintage aerial photo features to evaluate the completeness and accuracy of the baseline fault map and served as a guide for subsequent field reconnaissance. Many “features” were plotted that did not correspond to any known faults. Features that were consistently observed across the various image platforms suggested the location of previously unmapped faults or corroborated and helped relocate other faults.

Limited field reconnaissance and mapping helped to further refine the baseline fault map, confirming or refuting some interpreted faults. In some field locations additional geomorphic evidence of faulting was recorded that had not been observed in any of the imagery.

Two baselines of data are needed to compare the utility of the various image types. First is a baseline of the faults as previously mapped and presented in the published literature. Improvements in fault mapping are judged against this base. Second is a map of revised fault locations against which to judge the efficacy of each of the individual image types. The latter maps were derived from the previous mapping, as revised to correspond with the more definitive evidence from this study (including both image interpretation and field reconnaissance).

Accepting the final revised fault locations as a best approximation of the actual fault pattern, we then measured how many lineal meters of the fault traces had been identified in each image set. Conclusions are drawn from comparison of the relative utility of each image type for interpreting faults in a variety of terrain and vegetation conditions.

C. Original Mapping

The fault traces depicted on Figures 2a and 2b are the most recent published mapping of the San Andreas Fault Zone within the selected detail study areas. Fault labels indicated in parentheses below correlate to the labels on these two figures. The sources of these fault traces are as follows:

Indio – *Figure 2a (parenthetical fault labels are introduced for this study and are not from the original sources)*

- Principal trace (**SAF**) – mapped in various locations by Popenoe (1959), Hope (1969) and Clark (1984), we have taken the trace by Clark (published at 1:24,000) as the most recent and best published trace. The State's Alquist-Priolo map traces (California Division of Mines and Geology, 1974) are based on the earlier mapping and were not used for this comparison.
- Parallel trace (**SAF-nw-a**) – a minor sub-parallel trace from Keller and others (1982)
- North Branch (**SAF-NB**) – fault trace from Keller and others (1982)*
- Secondary trace (**SAF-Hope**) – from Hope (1969)
- Secondary trace (**NB-a**) – from Keller and others (1982)

** The mapping published by Keller and others (1982) was largely from an unpublished thesis by Bonkowski (1981). The map from this thesis is presently unavailable for comparison.*

Yucaipa – *Figure 2b (parenthetical fault labels are introduced for this study and are not from the original sources)*

- Principal trace (**SAF-1**) – from Matti and others (2003) and similar to California Division of Mines and Geology (1979). Within the northwestern block of the study area this trace separates crystalline bedrock on the northeast from Quaternary fan deposits on the southwest and then extends southeast across the Mill Creek floodplain and landslide terrain in the southeastern block.
- Sub-parallel trace (**SAF-2**) – a fault trace from Matti and others (2003) and California Division of Mines and Geology (1979), traverses varied terrain southwest of the principal trace.
- Secondary splay (**SAF-3**) – this trace from Matti and others (2003) crosses from SAF-1 to SAF-2 in the northwestern block.
- Secondary splay (**SAF-4**) – this inferred trace from Matti and others (2003) crosses from SAF-1 to SAF-2 within the Mill Creek floodplain.
- Secondary splay (**SAF-4alt**) – this inferred trace from California Division of Mines and Geology (1979) would appear to be an alternate location for SAF-4.
- Sub-parallel trace (**Fault A**) – this fault trace from Matti and others (2003) and California Division of Mines and Geology (1979) cuts crystalline terrain in the northwestern block and projects as an inferred fault (California Division of Mines and Geology, 1979) under the Mill Creek floodplain.
- Secondary splay (**Fault B**) – this trace from Matti and others (2003) cuts crystalline bedrock and truncates a Quaternary fan unit in the northwestern block.

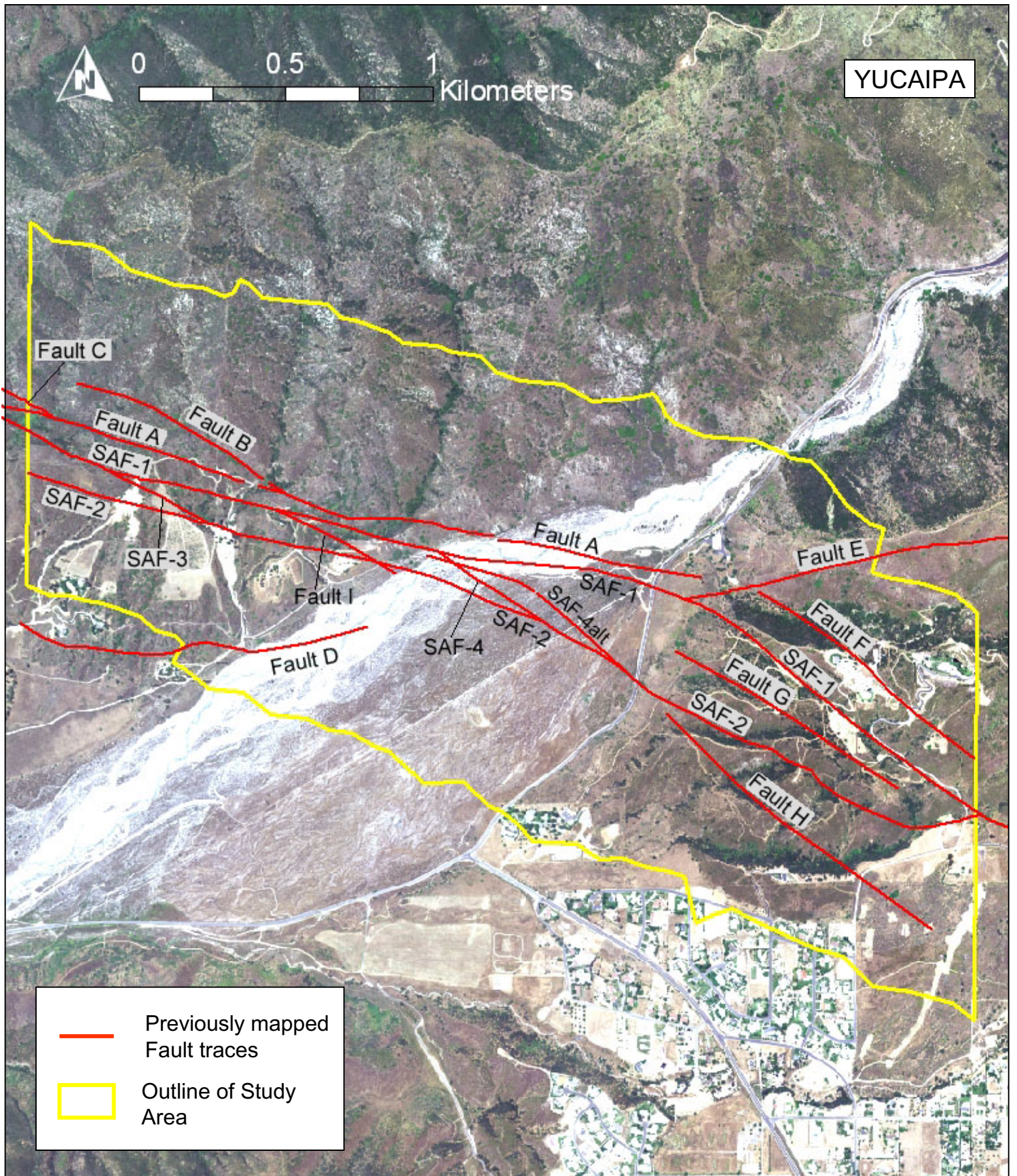


Figure 2b. Yucaipa study area showing previously mapped fault traces. See text (Section C) for explanation of fault labels and sources.

- Secondary splay (**Fault C**) – this splay from Matti and others (2003) joins fault A in the northwestern portion of the study area.
- Secondary thrust (**Fault D**) – this thrust fault from Matti and others (2003) is just barely covered by LiDAR imagery, and at that only within the Mill Creek floodplain. It was not evaluated in this study.
- Secondary splay (**Fault E**) – this oblique inferred splay from Matti and others (2003) had only equivocal expression in landslide terrain of the southeastern block and was not evaluated in this study.
- Sub-parallel trace (**Fault F**) – this trace from California Division of Mines and Geology (1979) crosses landslide terrain of the southeastern block.
- Sub-parallel trace (**Fault G**) – this trace from California Division of Mines and Geology (1979) crosses landslide terrain in the southeastern block.
- Sub-parallel trace (**Fault H**) - this trace from California Division of Mines and Geology (1979) crosses landslide terrain in the southeastern block.
- Secondary trace (**Fault I**) - this trace from California Division of Mines and Geology (1979) crosses between SAF-1 and SAF-2 in the northwestern block.

D. Setting

The two study areas are located along sections of the San Andreas Fault Zone in southern California (Figure 1). They differ from each other in geologic, geomorphic and vegetation details that provide a comparative test of the imagery used in different circumstances.

The Indio study area lies just south of where the southern San Andreas Fault splits into northern (Coachella) and southern (Banning) strands. Traces of the fault are found partly along the abrupt southwestern front of the Indio Hills and project southward beyond the hill front into more subdued desert terrain (Figure 2a). Some of this area has been significantly modified by human activity. Secondary fault strands lie within the uplifted terrain of the Indio Hills. Lithologic variation within the area is limited, with the main contrast corresponding to the topographic front. The Indio Hills in this locale are underlain by uplifted and highly folded terrestrial sediments of the Pleistocene Palm Spring Formation. Hills and ridges are capped by the more gently deformed Ocotillo Conglomerate. Vegetation is sparse, with occasional palm trees and palm oases being the only significant vegetation that might obscure the ground morphology.

The Yucaipa study area lies along the San Bernardino strand of the San Andreas Fault. This area includes three contrasting terrains (Figure 2b). The northwestern area, or block, presents faulting across uplifted bedrock terrain. The principal trace separates crystalline bedrock on the northeast from Quaternary sedimentary deposits on the southwest (Matti and others, 2003). Secondary traces traverse both bedrock types. In contrast, the southeast area, or block, is characterized by multiple fault strands across a landscape modified by large-scale mass movement. Landslide deposits are derived from the Tertiary non-marine Mill Creek Formation, northeast of the fault (Matti and others, 2003). The northwest and southeast areas are separated by the broad and relatively youthful Mill Creek floodplain. Vegetation varies from grasses to medium to dense chaparral and is densest in the southeastern block.

E. Remote Sensing Imagery

Imagery Acquisition

Six different types of imagery were acquired for this study that include standard black and white aerial photographs, LiDAR digital elevation model, ADS40/NAIP color ortho-image, ADS40/ISTAR color-infrared ortho-image, ADS40 Stereo imagery, and ASTER imagery. These imagery types are briefly described below and summarized in Table 1.

1. Aerial Photographs: Black and white aerial photos of different vintages (1930 and 1953/54) and scales (~1:18,000 and 1:20,000 respectively) are available at the California Geological Survey's (CGS) photo library or were borrowed from the U.S. Geological Survey.

Indio study area:

<u>Spence Airplane Photos</u>	black and white	7"x9"
4/16/30 1:18,000	negative numbers	180 to 185
<u>U.S. Department of Agriculture</u>	black and white	9"x9"
12/13/53 1:20,000	AXM-14K-129 to AXM-14K-132	
01/22/54 1:20,000	AXM-16K-46 to AXM-14K-49	

Yucaipa study area:

<u>Spence Airplane Photos</u>	black and white	7"x9"
4/16/30 1:18,000	negative numbers	113 to 118
<u>US Department of Agriculture</u>	black and white	9"x9"
02/16/53 1:20,000	AXL-42K-80 to AXL-42K-82	
02/16/53 1:20,000	AXL-43K-79 to AXL-43K-81	

2. LiDAR Digital Elevation Models (DEM): LiDAR (Light Detection And Ranging) DEM was downloaded from the GEON Grid Portal which is now incorporated in the Open Topography Portal of the GEON project. This topography data is part of the B4 campaign that covered most of the southern San Andreas Fault Zone in 2005 (Bevis and others, 2005). For this study, 0.5-m grid resolution, 1-m search radius, minimum elevation value of points, and Arc Grid format were specified from the portal's local binning algorithm for the DEM generation.

3. ADS40/NAIP Color Orthoimage: The ADS40 (Aerial Digital Sensor) camera system developed by Leica Geosystems was used in collecting 1-m ground sample distance (GSD), natural color ortho-images for the State of California as part of the U.S. Department of Agriculture's National Agriculture Imagery Program (NAIP). This dataset, which was processed using ORIMA software, is made available to state agencies as Digital Orthophoto Quarter Quads (DOQQ) in both ESRI Binary Grid (ADF) and GeoTIFF formats.

IMAGERY (Acquisition Date)		Format/Coverage	Scale/GSD	Stereo	Rectified	Geolocated	Estimated/ Stated Hor. Accuracy	Spectral Bands	Unique Characteristics	File Format	Projection/ Datum
1	Aerial Photos (1930,1953/54)	B&W Film/Paper 9 inch	~ 1:18000 ~1:20000	yes	no	no	same as warped imagery	1	pre-development photos, familiar character, sub-meter resolution in stereo.	paper JPEG TIFF	UTM, z11N NAD-83
2	LiDAR DEM (2005)	Digital Swath = 0.8 mi Variable length	0.5 m	no	yes	yes	10-20 cms	1	very high resolution topo with foliage penetration, 3D view, variable source of illumination.	ADF	UTM, z11N WGS-84
3	ADS40/NAIP (2005)	Digital Quarter Quads ~16 mi ²	1.0 m	no	yes	yes	5-10 m	3 (R,G,B)	synoptic coverage, natural color, vegetation and cultural features.	ADF, TIFF	UTM, z11N NAD-83
4	ADS40/ISTAR (2003)	Digital ~3 mi ² tiles	0.5 m	no	yes	yes	1.5 m	3 Pan 4 RGB/NIR	visible and near infrared, vegetation type, soil saturation.	FLT, ADF, TIFF	UTM, z11N NAD-83
5	ADS40 Stereo (2005)	Digital 5 mi x 100 mi (stereo subsets can be extracted using Leica GPro)	1.0 m	yes	partial	yes	6.0 m	5 (Pan,R,G,B, NIR)	rapid imagery interpretation with feature collection and attribution in stereo, variable vertical exaggeration.	TIFF	LSR Anchored WGS-84
6	ASTER (2006)	Digital ~38 mi ² /scene	15 m 30 m 90 m	yes no no	no no no	yes yes yes	~25 m	3 VNIR 6 SWIR 5 TIR	spectral information can be transformed into other forms or space	HDF, TIFF	UTM, z11N WGS-84

Table 1. Summary of properties and characteristics of the acquired imagery.

4. ADS40/ISTAR Infrared Ortho-image: The ISTAR ortho-images were collected by EarthData for California Office of Emergency Services and the Federal Emergency Management Agency following the 2003 fires in southern California. The ADS40 camera system, similar to that used for the NAIP imagery, was also utilized in this data collection. However, the more sophisticated ISTAR processing software package was used, resulting in a color infrared (CIR) image with a 0.5-m GSD and a 1.5-m horizontal accuracy. This imagery covers only the Yucaipa study area and was available in ESRI's floating point (.flt) file format.

5. ADS40 Stereo Imagery: In addition to the nadir-looking multispectral bands used to prepare the color ortho-images for NAIP, the ADS40 camera system also collects forward- and backward-looking imagery that can be used to create digital photogrammetric stereo images. In 2007, CGS purchased statewide digital stereo imagery prepared as part of the 2005 NAIP ortho-image production. A single stereo pair of images is comprised of one panchromatic image and either one natural color or another panchromatic image recorded by the same camera at a different look angle. These images have a 0.76 to 0.87 GSD and approximately a 6-m horizontal accuracy.

6. ASTER Imagery: ASTER (Advanced Spaceborne Thermal Emission and Reflection) multispectral imagery was downloaded from the LP DAAC EROS Data Center (<https://lpdaac.usgs.gov/>). This imagery consists of 14 bands (3 Visible and Near-Infrared, 6 Short Wave Infrared, and 5 Thermal Infrared) at 15-, 30-, 90-m GSD, respectively. The satellite scene was acquired in 2006 and is in Hierarchical Data Format and ADF formats.

Imagery Preparation and Processing

In order to undertake a comparative analysis of the suitability of the different imagery for fault trace mapping, it is imperative that they are in a format that can be displayed, overlaid, analyzed, and digitized in a Geographic Information System (GIS) environment. It is essential therefore that the various imagery have the same areal extent or have overlap, are georeferenced and co-registered, and have compatible file formats. Since the imagery acquired for this study was available in a variety of file formats, pixel sizes, areal coverages, and coordinate systems, considerable preparation and processing had to be undertaken. Additionally, derivative imagery was extracted from the acquired imagery and combination imagery was also generated by data fusion. Data fusion requires re-sampling, contrast stretching and re-projection.

The bulk of the image preparation (mosaicking, subsetting/trimming, projection, warping, etc.) and geoprocessing (topographic modeling, transformation, layer stacking, data fusion, etc.) was carried out using two very versatile GIS/Imagery processing software packages: **ESRI ArcGIS** (version 9.3) and **ITT ENVI** (version 4.4). An extension of ArcGIS, ERDAS Stereo Analyst for ArcGIS (**SAfA**) was used to handle the ADS40 Stereo imagery and a specialized software, **Leica GPro** (version 3.3), was used

to slice the stereo imagery strips into much smaller slices while retaining its usability on a GIS platform (McCrink, 2010). Occasionally, when rapid viewing and exchange of data were needed, data layers were converted into kmz files and viewed on **Google Earth Pro** (version 5.1).

Processed/Derived Imagery

The processed/derived imagery (summarized in Table 2) used in the actual fault interpretation and evaluation are:

- **Aerial Photographs** – paper prints from multiple years and at scales ranging from 1: 12,000 to 1:18,000 were interpreted and then scanned, mosaicked, trimmed, and warped for comparison with other images.
- **LiDAR DEM Shaded Relief** – derived from the DEM (mosaicked and trimmed), with two sources of illumination (45° azimuth/45° elevation and 225° azimuth/20° elevation). This imagery is considered the most accurately located geographic reference (UTM Zone 11N WGS84) for the study areas, hence the other imagery were projected to this coordinate.
- **ADS40/NAIP True Color Composite and False Color Composite**– trimmed and projected.
- **ADS40/ISTAR Color Infrared** – trimmed and projected.
- **ADS40 Stereo** – sliced into 6 x 9 km tiles. Look angles: Nadir, 16° forward and 14° backward for Yucaipa study area; Look angles: Nadir, 28° forward and 14° backward for Indio area. Various combinations of look angles were used to adjust vertical exaggeration to match the ruggedness of the area being interpreted. A color stereo image is realized when using the RGB image as one part of the stereo pair.
- **ASTER VNIR** – only the 15-m visible and near infrared (VNIR) bands were used in this study.
- **COMBINATION IMAGERY** – multispectral imagery are combined with LiDAR either by draping or data fusion:

Draped over LiDAR DEM Shaded Relief (draped imagery opacity set to 40%)

- ADS40/NAIP Color

ACQUIRED UNPROCESSED IMAGERY	IMAGERY PROCESSING/ TRANSFORMATION														DERIVED / PROCESSED IMAGERY		
	Scan	Mosaic	Warp	Georeference	Subset	Resample	Re-Project	Enhance	Contrast Stretch	Band Order	Topo Modeling	Layer Stacking	Data Fusion	Slice - GPro	Single	Combination	
																Draped over LiDAR DEM Shaded Relief	Fused with LiDAR DEM
Aerial Photos	x	x	x	x	x		x	x							Digital Aerial Photos		
LiDAR DEM		x			x			x			x				LiDAR DEM Shaded Relief		
ADS40/NAIP					x	x	x	x	x		x	x	x		ADS40/NAIP TCC	ADS40/NAIP TCC	ADS40/NAIP TCC
					x	x	x	x	x	x	x	x	x		ADS40/NAIP FCC	ADS40/NAIP FCC	ADS40/NAIP FCC
ADS40/ISTAR					x		x	x	x		x	x	x		ADS40/ISTAR TCC	ADS40/ISTAR TCC	ADS40/ISTAR TCC
					x		x	x	x	x	x	x	x		ADS40/ISTAR FCC	ADS40/ISTAR FCC	ADS40/ISTAR FCC
ADS40 Stereo								x						x	ADS40 Stereo		
ASTER					x	x		x	x	x	x	x	x		ASTER VNIR	ASTER VNIR	ASTER VNIR

TCC - True Color Composite FCC - False Color Composite

Table 2. Summary of the various image processing techniques used to generate the processed/derived imagery.

- ADS40/ISTAR Color Infrared
- ASTER VNIR

Fused with LiDAR DEM (Data Fusion was carried out in ENVI utilizing “Layer Stacking” and “Hill Shade” tools to transform the ADS40/NAIP color image into hue, saturation, value space. The value band is replaced with a shaded relief image that was calculated from the LiDAR DEM using various combinations of sun azimuth and sun elevation angle and utilizing bilinear resampling. The color image is transformed back to RGB space. The resulting image inherits the LiDAR 0.5-m higher resolution).

- ADS40/NAIP True Color Composite
- ADS40/NAIP False Color Composite
- ADS40/ISTAR Color Infrared
- ASTER VNIR

The width of the LiDAR imagery swath provided the lateral limits of coverage to which other imagery was adapted, as interpretation was only done within these limits. Graphic displays of some the processed/derived imagery used in the fault interpretation are shown in Figure 3a (Indio study area) and Figure 3b (Yucaipa study area).

Imagery Visualization and Analysis

General Observation of Features

Regardless of imagery type or platform, an effort was made to record every feature that might indicate the presence of an active fault. These included topographic features such as scarps, faceted spurs, benches, troughs, linear hill-fronts, and offset topographic features (such as drainages and ridges). Other drainage-related features, such as linear drainages, beheaded drainages, closed depressions, ponded alluvium and changes in drainage gradient or pattern were interpreted. Non-topographic features were also noted, such as tonal and vegetation contrasts or lineaments, or anomalous riparian growth. Marked truncations of the underlying geology, as indicated by geomorphology or surface tone or texture, were mapped. An effort was made in most platforms to observe features across the full width of the study area (as defined by the LiDAR swath), not just along the known fault traces, in order to possibly detect unmapped faults.

Mirror Stereoscope

Vintage aerial photographs were viewed as stereo pairs under a tabletop mirror stereoscope (Sokkisha MS27) using the standard accommodating lenses and 3x binocular lenses. They were also viewed at 4x magnification under an Abrams 2-4

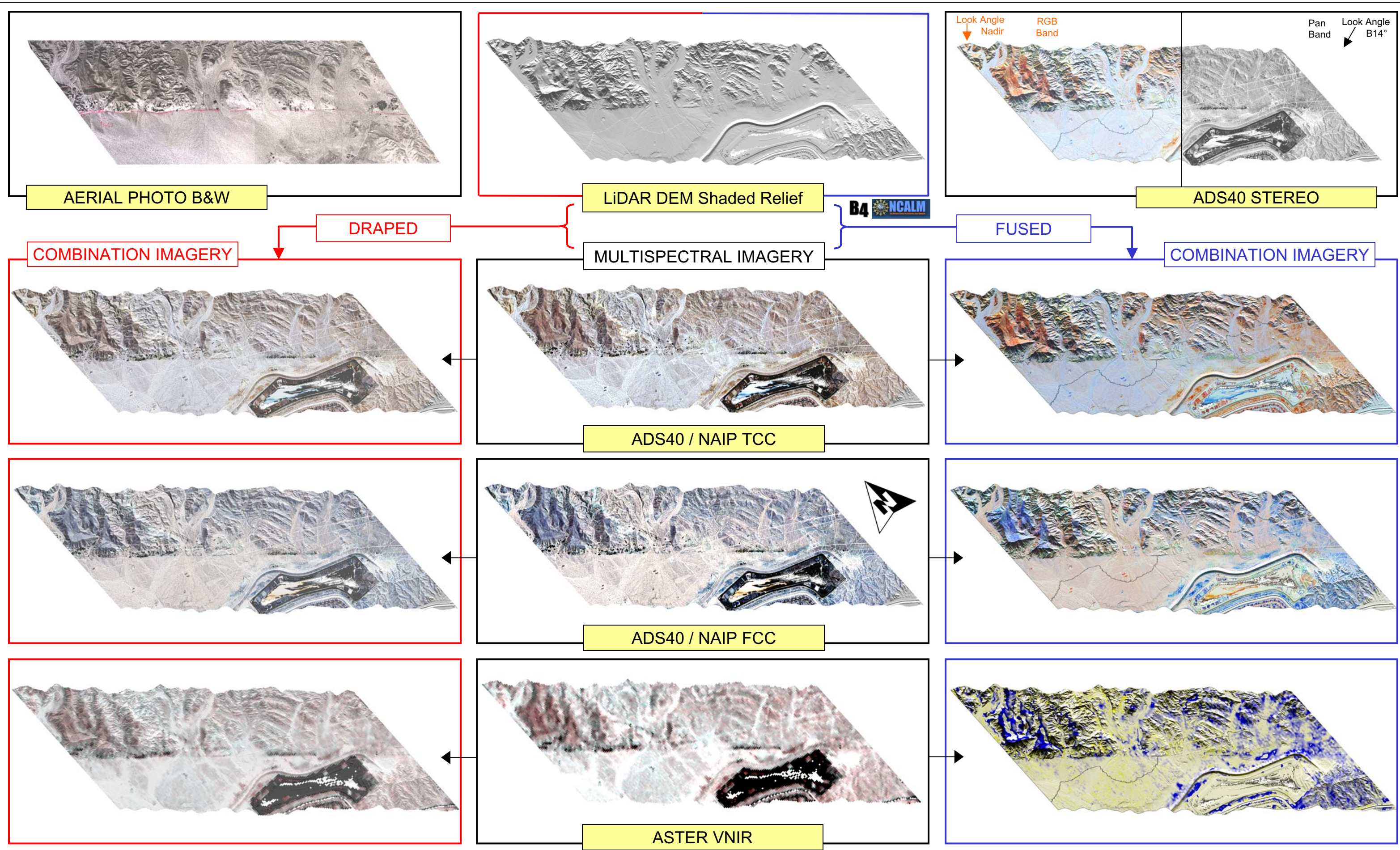


Figure 3a. Graphic displays of some of the processed / derived imagery used in the fault interpretation for the Indio study area..

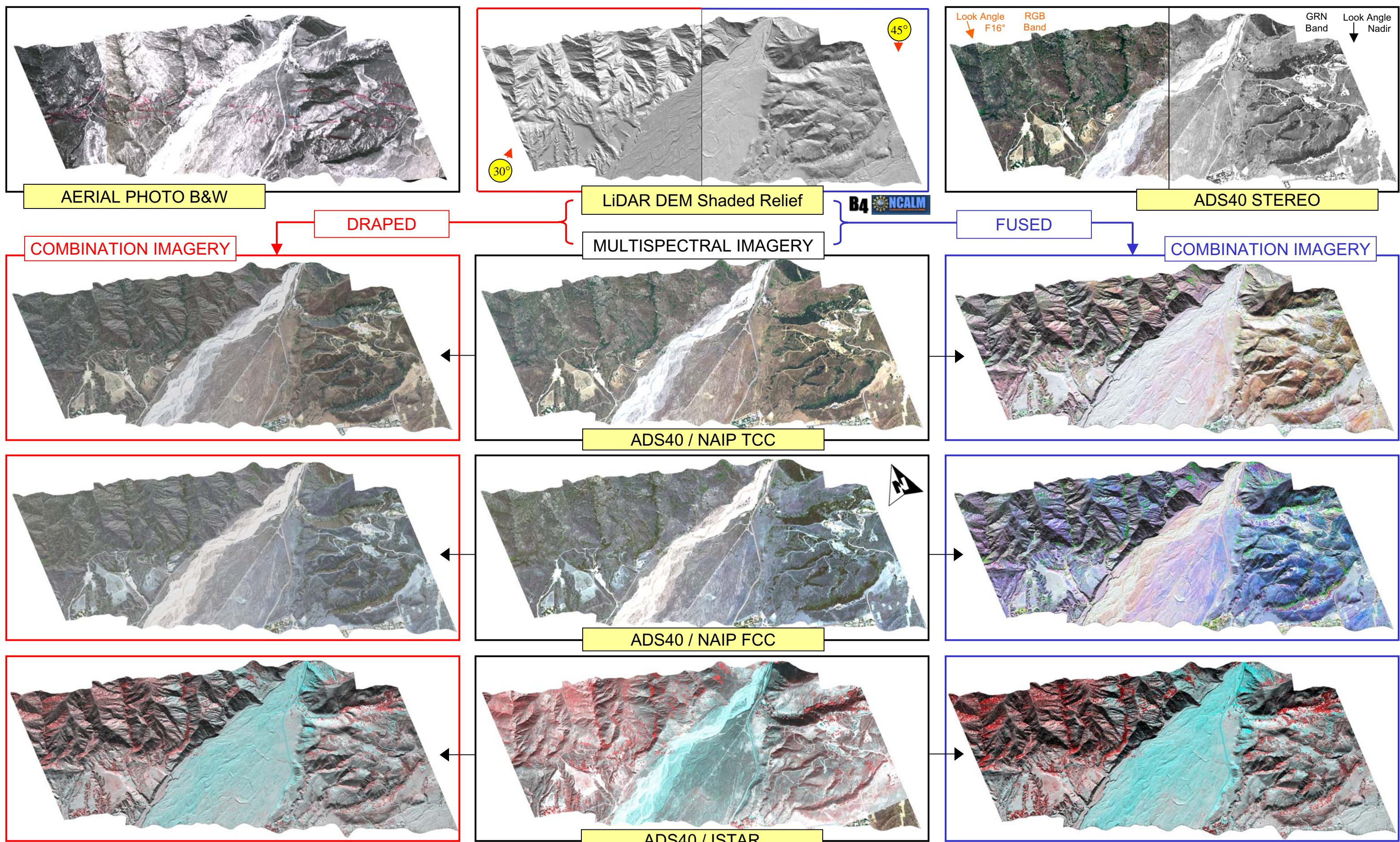


Figure 3b. Graphic displays of some of the processed / derived imagery used in the fault interpretation for the Yucaipa study area..

stereoscope. Interpreted features were plotted over the stereo model on one frame of the stereo pair. These interpreted images were scanned in sections and warped to a best fit of the true landform (as represented by the LiDAR DEM shaded relief) using MapInfo (v9.0) software. At this point all interpreted features were digitized in MapInfo. Due to the lack of orthographic projection of most of the vintage imagery this required repeated re-alignment of the scanned image for adjacent sub-areas. A separate interpretative layer was created for each of the aerial photo sets (1930 and 1953/54). Some features were seen in both flights and some were only interpreted from one or the other.

Due to imprecision in both interpretation and digitization the same feature seen on two sets of aerial photos was frequently plotted in two different locations as much as 10-20 meters apart. These were subjectively compared and realigned to create one complete, non-repetitive set of aerial photo interpretation for comparison with other imagery results. This compilation and adjustment was done over the LiDAR DEM shaded relief so that, where possible, the features could be located accurately on a corresponding feature in the LiDAR DEM shaded relief.

The interpreted traces and associated features were then imported into the ARCGIS geodatabase for further analysis and comparison with other data. More weight was given in analysis to features that formed a common alignment with each other or that correlated to features interpreted in other platforms. Less weight was given to single features or those that could be related to non-fault causes.

GIS Workstation

Each imagery type was viewed on the GIS workstation at a variety of scales to better detect large and small-scale features. For draped images we experimented with different levels of transparency to optimize the benefits of the LiDAR DEM being viewed with the addition of spectral elements from the other image. 40% transparency seemed optimum for the processed images that we used. Different illumination directions were also applied to the LiDAR DEM. Interpreted features were digitized with distinct line types being assigned to different feature types. Most interpretation was done independently of previous image results and an attempt was made to look beyond where features were expected. Nevertheless, some bias may have been inevitable based on what had been seen already in prior image interpretations. In a few instances where an image type did not appear very useful other image results were considered, as discussed in the Analysis and Discussion (Section G).

Stereo Workstation

The ADS40 Stereo imagery was displayed and analyzed in ArcGIS with the ERDAS Stereo Analyst (SAfA) extension, on a workstation equipped with E2 Emitter, Crystal Eyes glasses, TopoMouse 3D digitizing device, and NVIDIA Quadro FX4500 video card. Basic enhancements such as contrast and brightness were applied for best stereo viewing. Vertical exaggeration was also adjusted to match the ruggedness of the terrain by using different stereo pair combinations of image look angles. Other vector and raster data were used as references for the fault interpretations; vector data was converted into 3D features for display in the stereo environment, and both vector and raster data were displayed in the 2D map window while digitizing in 3D stereo.

Interpreted fault-related features were digitized in stereo and attributes were compiled in a structured database, which could then be compared to the data generated from the other imagery types.

Examples of the individual features mapped in six of the image sets for a small patch of the Yucaipa area are shown in Figure 4. These data, for the full extent of each study area (Figures 5a and 5b; Tables 3a and 3b, in Appendices), were used for fault interpretation and comparative analyses of imagery types.

F. Results

Figures 5a and 5b present a consolidated plot of all of the geomorphic features seen in each study area. These features were used, along with previous mapping and field reconnaissance, to refine the previous fault trace locations and, in some instances, infer newly mapped traces. Many of the features were observed in more than one image, in which case a judgment was made as to the best representation for the consolidated plot. Tables 3a and 3b (appendices) list each feature that was interpreted in the digital imagery along with relevant field observations and a matrix of which image types showed that particular feature. Features identified solely in the vintage aerial photography were not included in these tables.

Figures 6a and 6b show the reinterpreted faults used in this study for the comparison of the different image types. Tables 4a, 4b, 4c and 4d show the raw numbers indicating what percent of the presumed fault trace lengths were seen in each image type, for each of the two study areas. The totals for each area show that black and white stereo aerial photographs were most effective for mapping faults in either area, identifying 54% (Indio) to 50% (Yucaipa) of the accepted faults. In the sparsely vegetated Indio area ADS40 Stereo imagery was nearly as effective (53%) whereas in the chaparral-covered Yucaipa area LiDAR was the next most effective imagery (40%). However, these are gross comparisons and more can be learned by focusing on sections of faulting that share common characteristics. The discussion below is confined to the most useful imagery. The results from the other imagery are compiled in the tables.

For the Indio area (Figure 6a; Table 4a) we focused on seven fault sections including the principal trace of the San Andreas Fault (three sections), a significant northwest branch (two sections), and two additional splays.

Principal trace (SAF)

- **SAF-nw** – This section of the main trace consists of at least three sub-parallel fault strands that define the southwestern margin of the Indio Hills. These faults have locally sharp geomorphic expression and likely had displacement in the last major surface-rupturing earthquake. Vegetation is light to moderate (oases). In spite of the greater resolution of the LiDAR imagery, more of these traces (52%) were plotted on the ADS40 Stereo imagery. 40% were plotted in the interpretation of vintage stereo photographs, 35% in ADS40/NAIP and 34% on

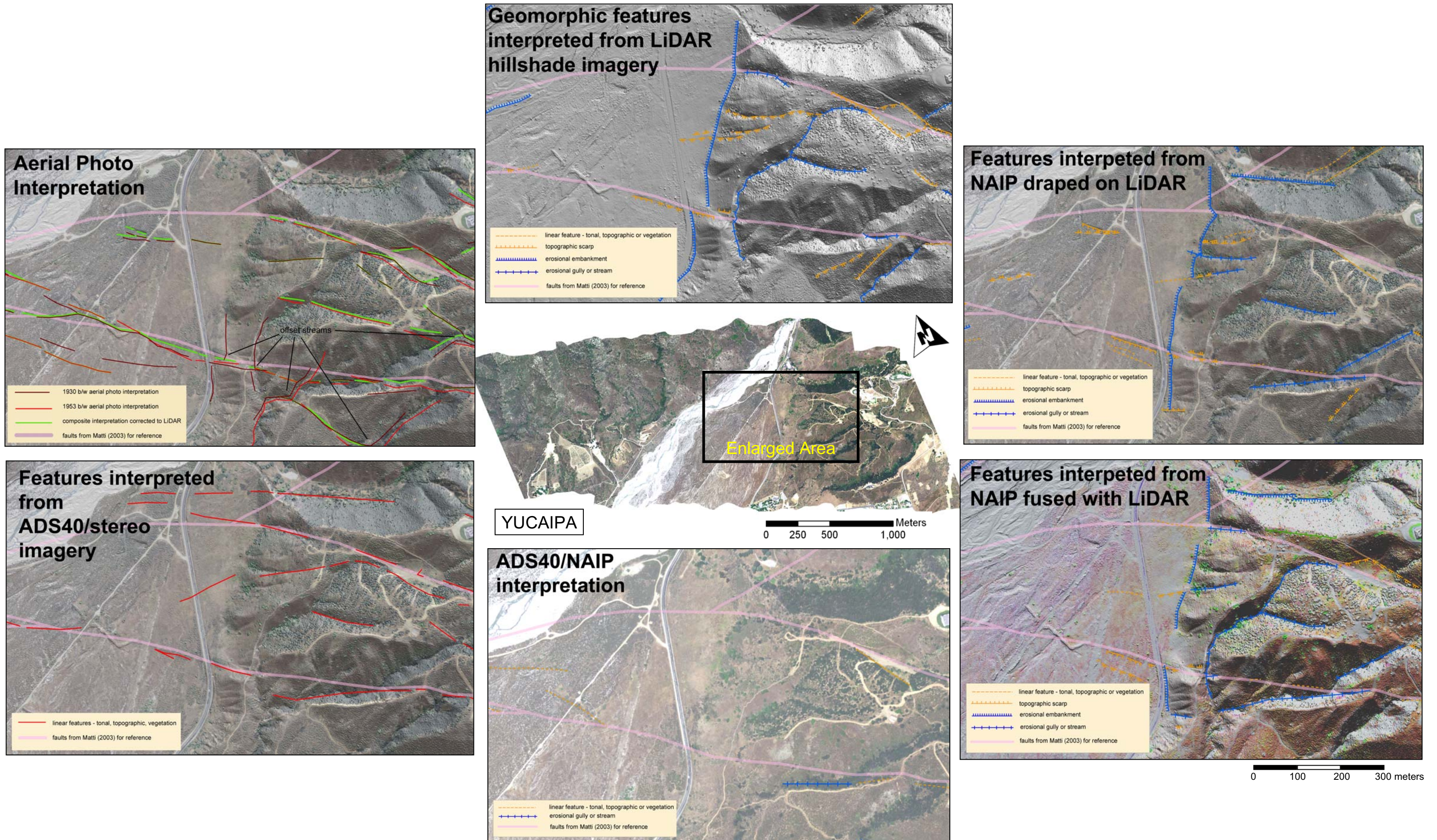
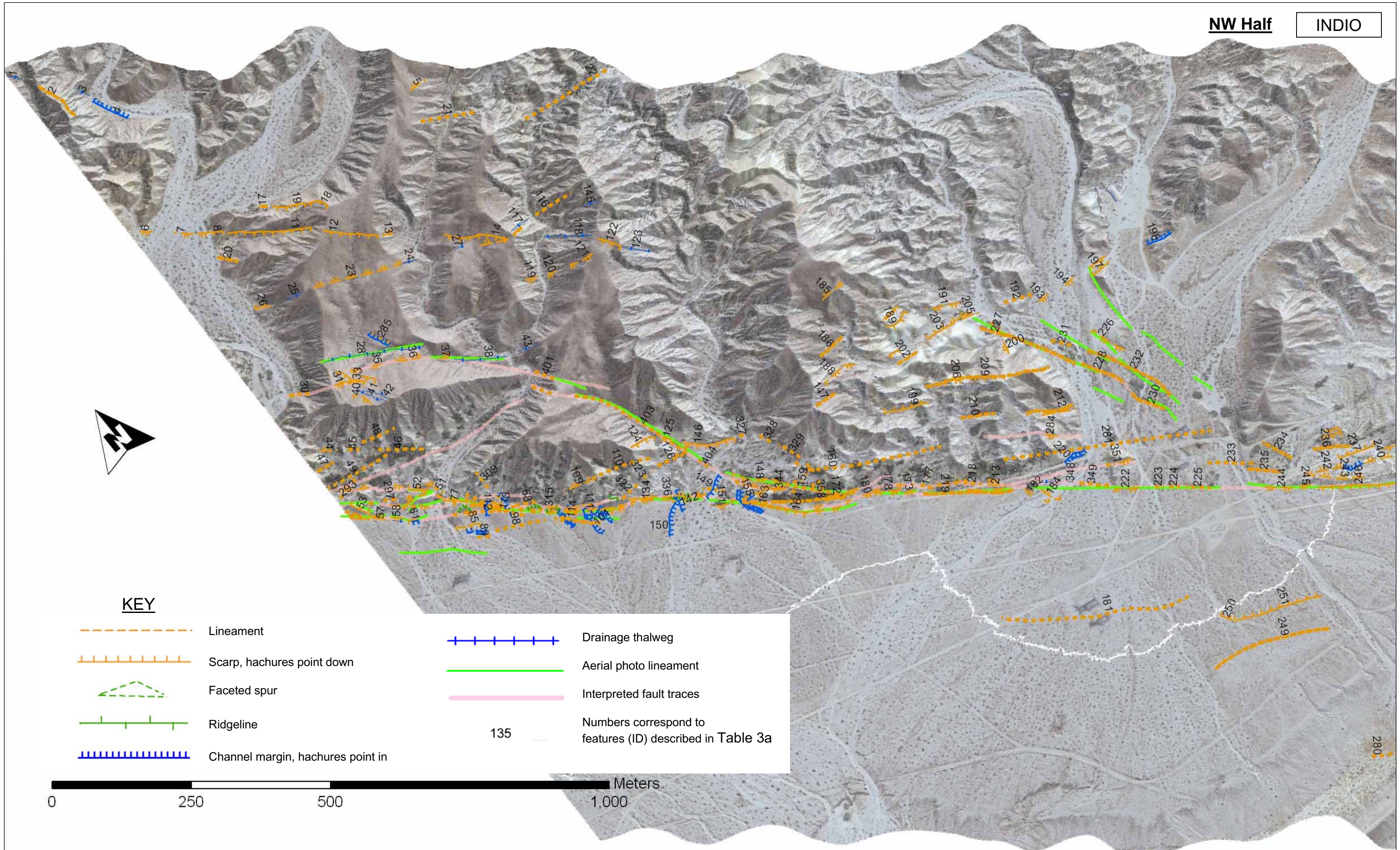


Figure 4. Examples of features mappable in different imagery and combinations. Examples are from the Yucaipa study area and span both floodplain and elevated terrain.



KEY

-  Lineament
-  Scarp, hachures point down
-  Faceted spur
-  Ridgeline
-  Channel margin, hachures point in
-  Drainage thalweg
-  Aerial photo lineament
-  Interpreted fault traces
-  Numbers correspond to features (ID) described in Table 3a

0 250 500 1,000 Meters

Figure 5a (NW Half). Consolidated plot of fault-related geomorphic features interpreted in the Indio study area.

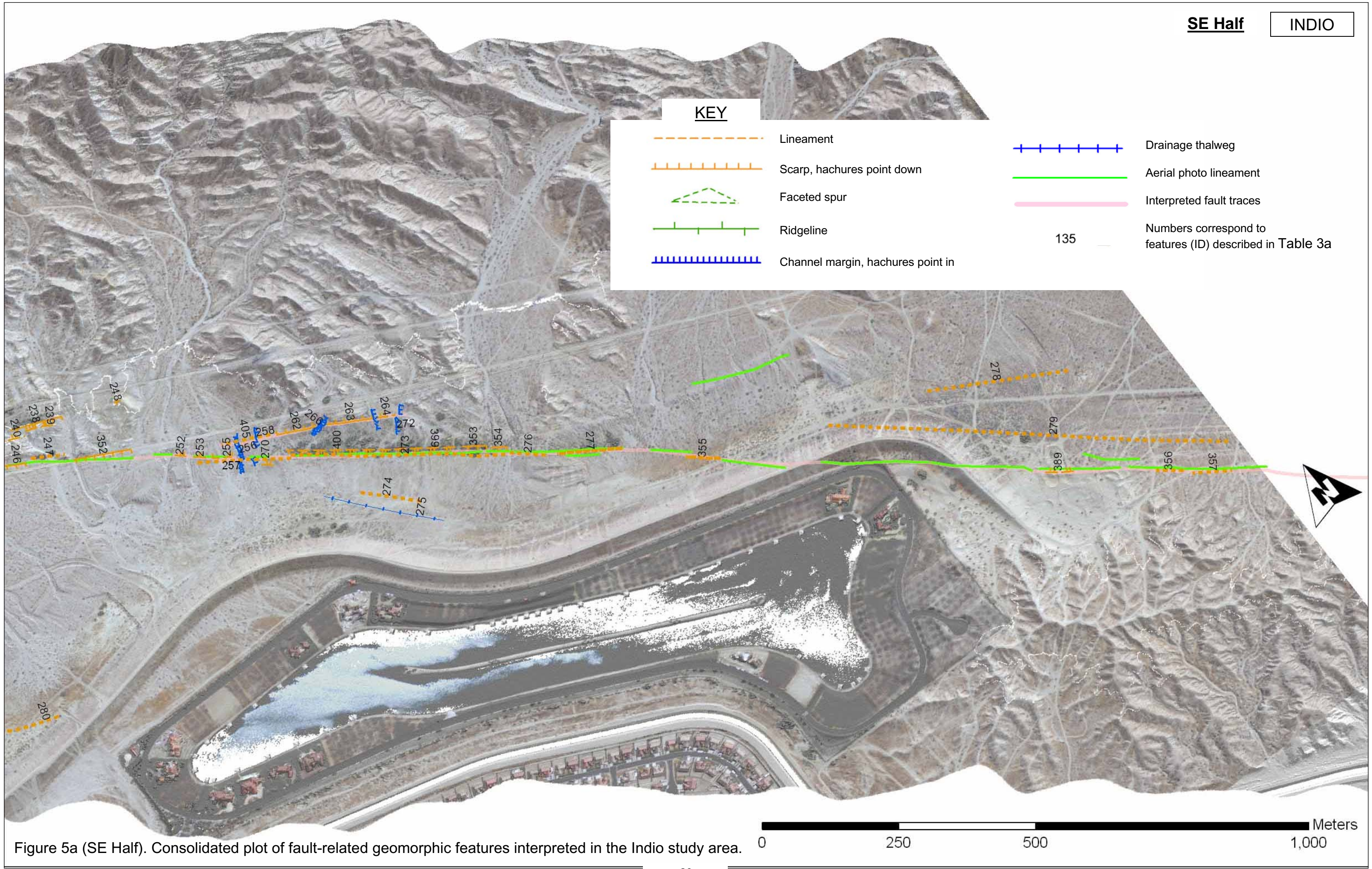


Figure 5a (SE Half). Consolidated plot of fault-related geomorphic features interpreted in the Indio study area.

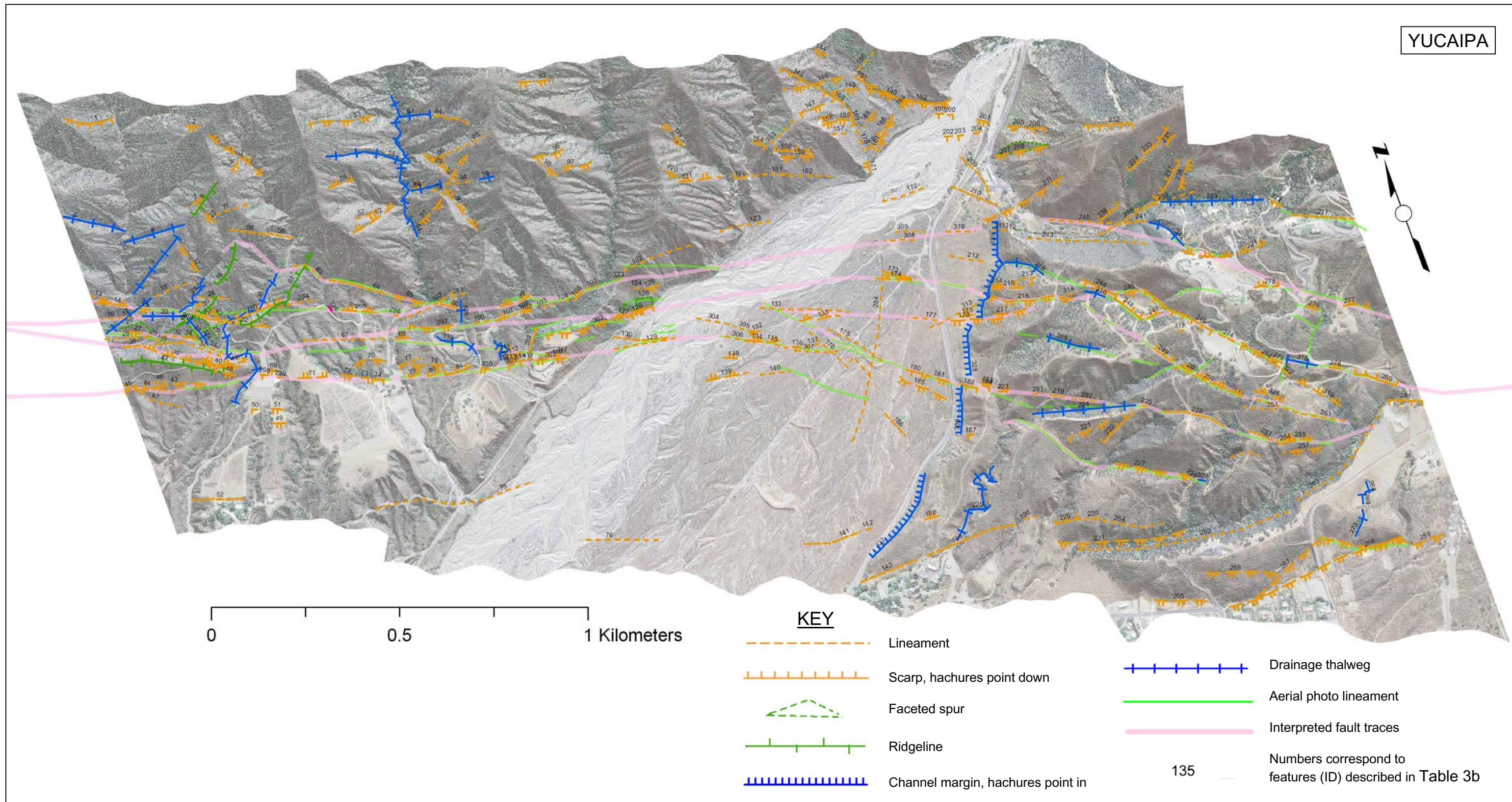


Figure 5b. Consolidated plot of fault-related geomorphic features interpreted in the Yucaipa study area.

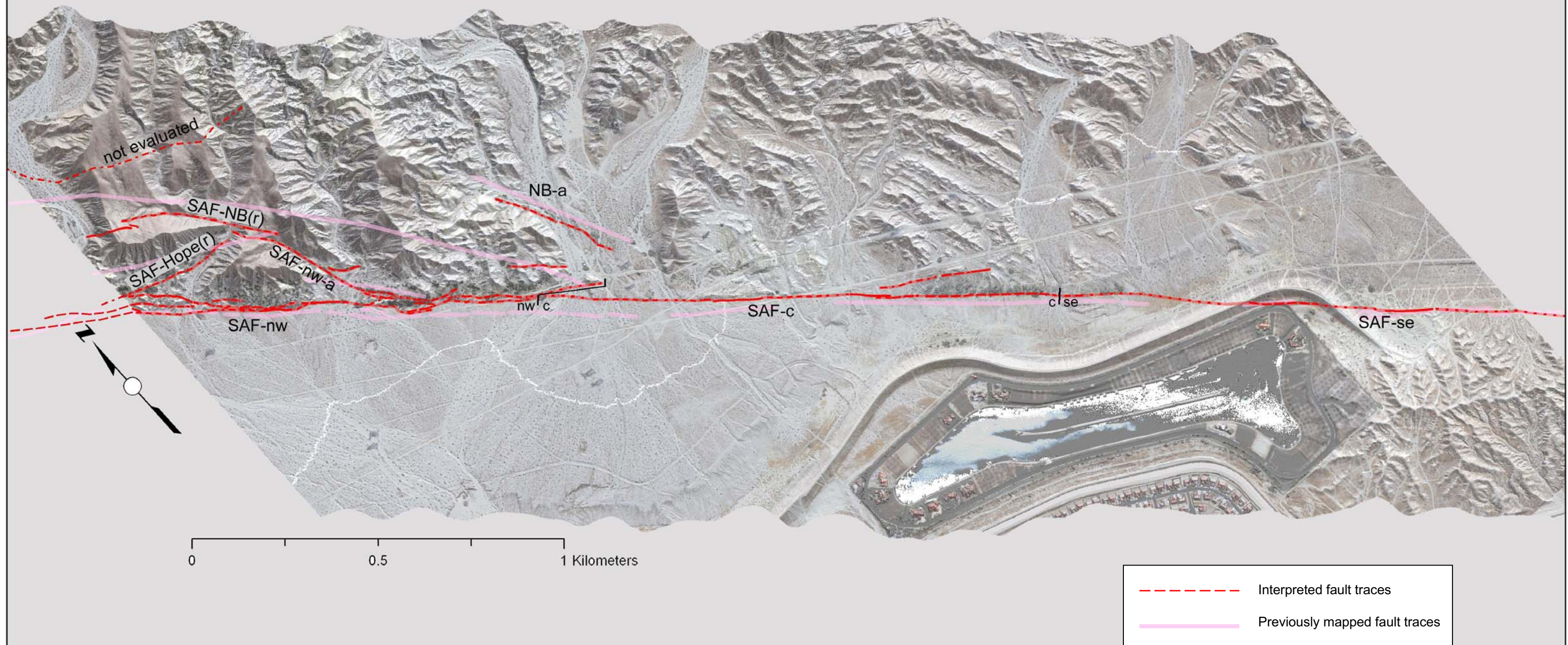


Figure 6a. Interpreted fault traces in the Indio area. See text (Section F) for explanation of fault labels. Previously mapped fault traces shown for comparison.

Indio study area

INTERPRETED FAULTS			PROPORTION (Length and Percentage) OF FAULT TRACES IDENTIFIED IN EACH IMAGERY TYPE															
Fault Trace	Geology	Length meter (m)	Aerial Photo		LiDAR DEM		ADS40/NAIP		ADS40 Stereo		ASTER		Draped on LiDAR		Fused with LiDAR DEM			
													ADS40/NAIP		ADS40/NAIP T		ADS40/NAIP F	
			m	%	m	%	m	%	m	%	m	%	m	%	m	%	m	%
SAF-nw	Qp/Qal	2425	970	40%	820	34%	860	35%	1260	52%	915	38%	480	20%	575	24%	620	26%
SAF-c	Qp/Qal	1735	1155	67%	925	53%	905	52%	1180	68%	1050	61%	960	55%	615	35%	795	46%
SAF-se	Qal	1245	1050	84%	105	8%	180	14%	365	29%	845	68%	180	14%	165	13%	185	15%
SAF-NB(r)	Qo, Qp	555	210	38%	75	14%	0	0%	175	32%	0	0%	140	25%	205	37%	0	0%
SAF-nw-a	Qo, Qp	845	425	50%	285	34%	190	22%	660	78%	150	18%	185	22%	135	16%	85	10%
SAF-Hope(r)	Qp	330	0	0%	0	0%	90	27%	15	5%	0	0%	0	0%	0	0%	0	0%
NB-a	Qal	345	225	65%	0	0%	300	87%	325	94%	295	86%	335	97%	225	65%	235	68%
Sum	%	7480	4035	54%	2210	30%	2525	34%	3980	53%	3255	44%	2280	30%	1920	26%	1920	26%

Qal - younger alluvium and fan deposits
 Qo - Ocotillo conglomerate
 Qp - Palm Spring Formation
 / - indicates one unit faulted against the other

T - True Color Composite
 F - False Color Composite

Table 4a. Interpreted faults in the Indio study area showing the proportion (length and percentage) of fault traces identified in each imagery type. See Figure 5a for fault trace locations.

the LiDAR DEM shaded relief. Although the percentages between the ADS40/NAIP and the LiDAR are similar, there were some fault elements seen by each that were not visible in the other imagery and some elements not even picked up in the ADS40 Stereo interpretation. *The greater resolution of the LiDAR did seem to allow a slightly more accurate location as well as the ability to better discern multiple traces that are close together.*

- **SAF-c** – This section of the main trace, while still bounding the Indio Hills, is for the most part a single trace that transects several broader alluvial surfaces with light vegetation. Interpretation of vintage stereo photographs and ADS40 Stereo imagery identified more than 67-68% of this fault section. ADS40/NAIP overlain on LiDAR DEM shaded relief allowed plotting of 55% of the fault section. However, either image alone did almost as well (52-53%). *This section demonstrated the benefit of true stereo to the interpretation.*
- **SAF-se** – This section of the main trace is almost entirely within an alluvial fan environment with light vegetation. Much of this trace has been obscured by historic modification of the land surface (power lines, roads, levees). As a result of the recent modification, vintage aerial photographs had a clear advantage, allowing the mapping of 84% of the fault in contrast to less than 30% for any of the modern imagery.

Northwest branch – within the Indio Hills

- **SAF-NB(r)** – This northerly fault trace probably helps distribute slip to the Coachella strand (North Branch) of the San Andreas Fault. This trace was relocated and re-interpreted in this study to join the principal trace a little further to the northwest of the trace mapped by Keller and others (1982). The trace mapped by Keller and others (1982) lacks any geomorphic expression, especially across several elevated fan surfaces where the fault should be visible. Vegetation is light. No single image type was superior for mapping this fault strand, with 38% plotted on vintage stereo photographs, 37% in ADS40/NAIP fused with LiDAR DEM and 32% in ADS40-Stereo imagery. It is notable that the various images were additive in this area, with each image identifying some parts not seen in the other images; as a set they identified nearly all of the fault. LiDAR alone only highlighted 14% of this fault segment.
- **SAF-nw-a** – This segment of the northerly branch was not previously mapped and is interpreted as an *en echelon* continuation of the Northerly branch. Where it approaches the main trace it includes a smaller fault segment mapped previously by Keller and others (1982). Vegetation is light to moderate (oases). This segment was well identified in ADS40 Stereo imagery (78%) while only 50% was mapped on vintage stereo photographs and only 34% was detected in the LiDAR DEM (principally where it runs close to the main trace). ADS40 Stereo imagery did particularly well in identifying parallel traces.

Additional Splays

- **SAF-Hope(r)** – This fault trace is relocated, from a trace mapped by Hope (1969), to coincide with a series of oases, truncated older fan surfaces and fault exposures in the unnamed canyon south of the fault. Other than the crude line of vegetation, this feature was not picked as a fault trace in most of the imagery. The vegetation lineament was a little better defined immediately to the northwest of the study area and might have provided a better basis for extrapolation if it had been considered. The feature is better located based on field mapping where shear zones and discontinuities in surfaces were more apparent.
- **NB-a** – This inferred trace, mapped by Keller and others (1982), is a prominently visible feature in all of the spectral imagery used (65-97% mapped). It was not noted in LiDAR, which is blind to soil color, but was seen when the LiDAR DEM was combined with color digital imagery. It is conformable with bedding, and field reconnaissance suggests that it is principally a zone of lithologic contrast that may have experienced some localized bedding-plane shear, but it could not be corroborated as a significant fault. Vegetation is light, with a few localized palms.

For the Yucaipa area (Figure 6b; Tables 4b-d) we looked at three principal sub-parallel fault strands and several more secondary faults or fault-like lineaments. What we judge to be the principal trace of the fault – SAF-1 – is the trace that separates crystalline bedrock on the northeast from Quaternary sediments on the southwest (Matti and others, 2003). Our discussion and analysis is subdivided along the distinct geologic/geomorphic subareas that characterize the Yucaipa area. The primary fault strands cross most or all of the study area and are therefore divided into sections that are discussed separately along with other faults within the same terrain.

Northwestern area – bedrock terrain (Table 4b)

- **SAF-1w** – This northwestern section of the main trace has been only slightly relocated from the mapping of Matti and others (2003) to coincide with fault-like morphology mapped in this study. The fault extends through terrain with mostly moderate chaparral vegetation. 46% of this fault section was mapped from the LiDAR DEM shaded relief and less than half as much was detected with other combinations of LiDAR and ADS40 images. Only 8% was seen in the ADS40 Stereo images, however most of this was not plotted in other imagery.
- **SAF-1ww** – This short fault strand has not been previously mapped and is inferred from an alignment of faceted spurs and other geomorphic features suggestive of faulting. The fault extends through terrain with mostly moderate chaparral vegetation. It was primarily detected in the vintage stereo photographs where 80% of it was mapped. Nearly 60% of the fault was also mapped in ADS40 Stereo imagery as well as in a combination of ADS40/NAIP imagery draped on the LiDAR DEM shaded relief. Only 43% of the fault was seen in LiDAR alone.

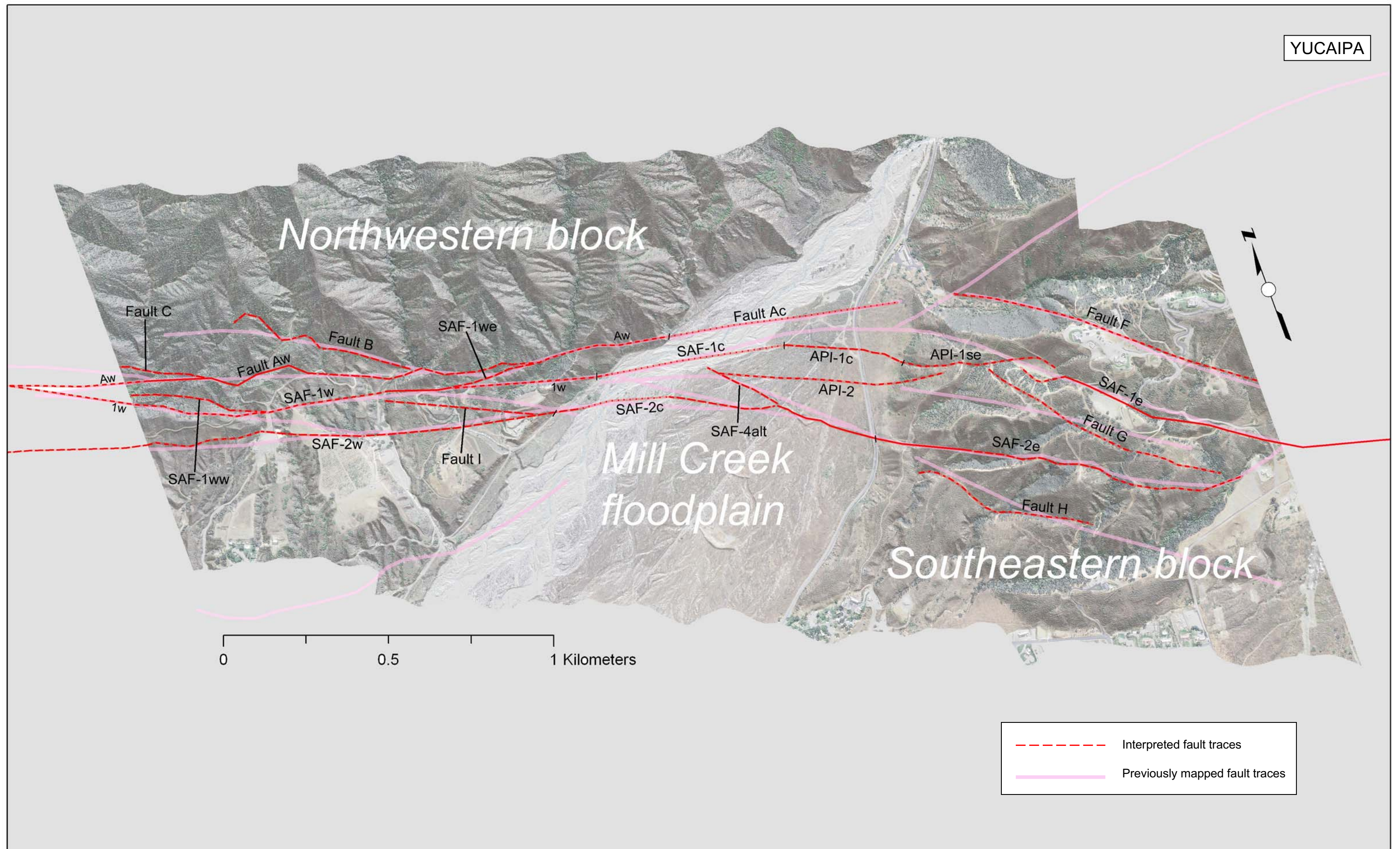


Figure 6b. Interpreted fault traces in the Yucaipa area. See text (Section F) for explanation of fault labels. Previously mapped fault traces shown for comparison.

Yucaipa study area

INTERPRETED FAULTS			PROPORTION OF FAULT TRACES (Length and Percentage) IDENTIFIED IN EACH IMAGERY TYPE																	
Fault Trace	Geology	Length meter (m)	Aerial Photo		LiDAR DEM		ADS40/NAIP		ADS40/ISTAR		ADS40 Stereo		Draped over LiDAR				Fused with LiDAR DEM			
			m	%	m	%	m	%	m	%	m	%	m	%	m	%	m	%	m	%

4b. Northwest area - bedrock terrain.

SAF-1w	gg/Qof,Qyf	1410	275	20%	650	46%	125	9%	0	0%	115	8%	345	24%	325	23%	90	6%	50	4%		
SAF-1ww	gg	415	330	80%	180	43%	0	0%	0	0%	240	58%	245	59%	0	0%	0	0%	190	46%		
SAF-1we	gg	275	280	102%	205	75%	125	45%	0	0%	215	78%	160	58%	0	0%	0	0%	35	13%		
SAF-2w	Qof, Qyf	1250	610	49%	450	36%	0	0%	0	0%	455	36%	375	30%	450	36%	540	43%	440	35%		
Fault Aw	gg, Qyf	1685	1200	71%	815	48%	470	28%	0	0%	840	50%	520	31%	105	6%	160	9%	215	13%		
Fault B	gg	600	240	40%	390	65%	150	25%	135	23%	330	55%	370	62%	180	30%	0	0%	0	0%		
Fault C	gg	270	145	54%	150	56%	0	0%	0	0%	0	0%	0	0%	0	0%	120	44%	0	0%		
Fault I	Qof, Qyf	455	340	75%	150	33%	0	0%	0	0%	0	0%	35	8%	85	19%	0	0%	25	5%		
Sum	%	6360	3420	54%	2990	47%	870	14%	135	2%	2195	35%	2050	32%	1145	18%	910	14%	955	15%	0	0%

Qyf - younger alluvial fan deposits
Qof - older alluvial fan deposits

gg - gneissic basement rock
/ - indicates one unit faulted against the other

T - True Color Composite
F - False Color Composite

4c. Central area - alluvial floodplain of Mill Creek.

SAF-1c	Qal	585	0	0%	380	65%	0	0%	0	0%	30	5%	50	9%	0	0%	0	0%	0	0%		
API-1c	Qoal	370	175	47%	0	0%	0	0%	0	0%	0	0%	140	38%	0	0%	0	0%	0	0%		
SAF-2c	Qal,Qoal	1000	730	73%	200	20%	90	9%	135	14%	410	41%	175	18%	80	8%	100	10%	100	10%	170	17%
Fault Ac	Qal,Qoal	710	0	0%	0	0%	0	0%	0	0%	175	25%	0	0%	0	0%	0	0%	0	0%		
Fault-API-2	Qoal	690	0	0%	220	32%	190	28%	255	37%	0	0%	325	47%	0	0%	275	40%	250	36%		
SAF-4alt	Qoal	240	190	79%	0	0%	65	27%	0	0%	0	0%	0	0%	0	0%	0	0%	0	0%		
Sum	%	3595	1095	30%	800	22%	345	10%	390	11%	615	17%	690	19%	80	2%	375	10%	350	10%	170	5%

Qal - young and modern stream channel deposits of Mill Creek
Qoal - older flood plain and channel deposits of Mill Creek

4d. Southeast area - landslide disturbed bedrock terrain

SAF-1e	landslide	840	725	86%	590	70%	170	20%	0	0%	565	67%	280	33%	0	0%	240	29%	370	44%		
API-1se	landslide	470	250	53%	420	89%	0	0%	0	0%	245	52%	115	24%	0	0%	260	55%	140	30%		
SAF-2e	landslide	1140	525	46%	535	47%	280	25%	40	4%	385	34%	410	36%	0	0%	405	36%	500	44%		
Fault F	landslide	960	340	35%	0	0%	0	0%	0	0%	125	13%	70	7%	0	0%	0	0%	175	18%		
Fault G	landslide	780	555	71%	350	45%	255	33%	0	0%	460	59%	190	24%	185	24%	445	57%	320	41%		
Fault H	landslide	570	510	89%	210	37%	195	34%	0	0%	210	37%	165	29%	205	36%	255	45%	275	48%		
Sum	%	4760	2905	61%	2105	44%	900	19%	40	1%	1990	42%	1230	26%	390	8%	1605	34%	1780	37%	0	0%

landslide deposits derived from Mill Creek Formation

Tables 4b, 4c, 4d. Interpreted faults in the Yucaipa study area showing the proportion (length and percentage) of fault traces identified in each imagery type.

See Figure 5b for fault trace locations.

- **SAF-1we** – This previously unmapped fault segment is inferred from a strong alignment of geomorphic features suggestive of faulting. The fault extends through terrain with light to moderate chaparral vegetation. It was interpreted in its entirety from vintage stereo photographs but is also strongly visible in ADS40 Stereo images (78%) and LiDAR (75%). Other image combinations tended to obscure what could be seen.
- **SAF-2w** – This second persistent trace of the San Andreas Fault, southwest of SAF-1, is inferred by Matti and others (2003) to be a reactivated trace of the Mission Creek Fault. It has been slightly relocated to correspond with some subtle geomorphic features. The fault extends through terrain with mostly light to moderate chaparral vegetation and grasses. Vintage stereo photographs showed features associated with almost 50% of this fault section. LiDAR and ADS40 Stereo were able to see only a little more than a third of the fault lineament, but not the same third as each other. About half of what was detected in LiDAR or ADS40 Stereo was not detected in the other. Also, a significant part of what was seen in the LiDAR DEM or ADS40 Stereo was not seen in the vintage stereo photos (about a quarter of the total fault length). ADS40/NAIP fused with LiDAR DEM did a little better (43%).
- **Fault Aw** – This fault trace from Matti and others (2003) lies within the crystalline bedrock terrain of the northwestern block, but locally truncates some Quaternary deposits. It has been relocated in some areas to correspond to offset streams and ridges as well as some more subtle geomorphic features. The fault extends through terrain with mostly light to moderate chaparral vegetation and grasses. Principally identifiable in vintage stereo photographs (71%), the location was also corroborated for roughly half of its length by ADS40 Stereo and LiDAR imagery. As with the SAF-2w strand, these latter two image sets each added their own unique segments of the fault for about two-fifths of their contributions and combined they detected several hundred meters of fault not seen in the aerial photography.
- **Fault B** – This short fault, originally from Matti and others (2003), lies even higher in the crystalline bedrock terrain and its trace has been adjusted to match probable fault morphology. It extends through terrain with light to moderate chaparral vegetation and grasses. 65% of the fault trace was detectable in the LiDAR DEM shaded relief and only 55% in the ADS40 Stereo imagery. Both of these image types did better than the 40% detection in vintage stereo photographs. NAIP draped on LiDAR DEM shaded relief led to almost as much fault length being identified as in the LiDAR alone, but the location did not seem as accurate.
- **Fault C** – This short fault segment has been shifted from its location as mapped by Matti and others (2003) to correspond to several subtle hillslope features visible through light to moderately dense chaparral. More than half of this fault

segment was detected in the LiDAR DEM or vintage stereo photographs. It was not seen in the ADS40 Stereo imagery.

- **Fault I** – This short fault is originally from the Alquist-Priolo Earthquake Fault Zone (APEFZ) map for the Yucaipa quadrangle (California Division of Mines and Geology, 1979). It is relocated to match features interpreted in this exercise. The fault extends through terrain with light to medium-dense chaparral vegetation. It is principally visible in the vintage stereo photographs (75%). Only 1/3 of it was detected in the LiDAR DEM shaded relief and it was not seen at all in the ADS40 Stereo images.

Central area – alluvial floodplain of Mill Creek (Table 4c)

- **SAF-1c/API-1c** – This central section of the main trace has been relocated from the concealed trace shown by Matti and others (2003). It has been shifted to follow some previously unmapped subtle features in the older floodplain deposits (API-1c) and to align with more prominent features in the southeastern block. Vegetation can be moderate on the older abandoned floodplain surfaces. Features seen in LiDAR imagery weakly support 40% of the fault trace where it may have controlled the margin of the most recent Mill Creek channel. 20% of the fault was suggested by ADS40/NAIP imagery draped on the LiDAR DEM shaded relief, much of this in the older portions of the floodplain. Upon reviewing the other imagery, the LiDAR alone appeared to reveal just as much of these lineaments in the older floodplain surface. Vintage stereo photographs picked up a few more of the features in the older surface (API-1c) but less elsewhere for about 18% of the fault.
- **SAF-2c** – This central portion of SAF-2 is slightly relocated from the concealed trace of Matti and others (2003) to match features observed within the floodplain of Mill Creek. Vegetation can be moderate on the older abandoned floodplain surfaces. 73% of this fault trace was supported by features in vintage stereo photographs. ADS40 Stereo imagery highlighted 41% of the inferred fault and LiDAR revealed only 20%.
- **SAF-4-alt** – This is an alternate location for the concealed fault (here designated SAF-4) of Matti and others (2003). The location depicted partially corresponds with a fault trace on the APEFZ map (California Division of Mines and Geology, 1979) and is further supported by some features observed in this study. The fault traverses lightly to moderately vegetated older alluvial surfaces. 79% of it was supported by features seen in vintage stereo photographs and about one quarter of it was suggested in the ADS40/NAIP imagery. It was not seen at all in LiDAR DEM or ADS40 Stereo.
- **Fault Ac** – This is the southeastern projection, by Matti and others (2003) of a fault that is more clearly identified in the bedrock terrain to the north. Its location across the floodplain is only marginally supported by a few subtle features. Vegetation is relatively light. This fault extension is not well supported by the

image analysis, only 25% of it being suggested by the ADS40 Stereo imagery and not at all by the other imagery.

- **Fault-API-2** – This previously unmapped inferred fault trace is based on features observed in this study. The fault traverses lightly to moderately vegetated older alluvial surfaces and continues for about 140 meters into the adjacent hillslope. The westernmost third of the fault was suggested by a weak vegetation lineament in the ADS40/NAIP and ISTAR imagery. The eastern part of the fault was indicated mostly by weak lineaments in draped or fused imagery, with less than a third of the trace supported by LiDAR data (mainly in the adjacent hillslope). It was not seen in any stereo images (photographic or digital).

Southeastern area – landslide disturbed bedrock terrain (presence of landsliding makes some interpretations equivocal) (Table 4d)

- **SAF-1e** - This southeastern section of the main trace has been relocated from the mapping of Matti and others (2003) to correspond with observed geomorphic features and to project to a more strongly supported fault trace to the northwest. Following an interpretation that the prominent rhombochasm along this trace is related to extensional faulting rather than landsliding we project the fault northwestward to join API-1. The fault lies within terrain covered by moderate to dense chaparral vegetation. 86% of this fault trace was located in vintage stereo photographs, 70% in LiDAR and 67% in ADS40 Stereo. Combinations of LiDAR and ADS40 imagery did not fare as well (44% or less).
- **API-1se** – This extension of API-1 into the southeastern block is based on an alignment of features observed in this study, principally LiDAR DEM (89% of the feature). 55% of it is suggested by ADS40/NAIP fused with LiDAR DEM and a little more than half of the segment is suggested by stereo interpretation (photographic or digital). Chaparral vegetation is moderate to dense.
- **SAF-2e** – This fault trace, from Matti and others (2003) is only slightly relocated to correspond to several features observed in this study. The fault lies within terrain covered by moderate to dense chaparral vegetation. 47% of the fault was located in LiDAR and 46% in vintage stereo photographs. Slightly less was seen in some LiDAR combinations and ADS40 Stereo images showed only 1/3 of this trace.
- **Fault F** – This inferred fault trace, from California Division of Mines and Geology (1979) is only slightly relocated to correspond to limited features observed in this study. The fault lies within terrain covered by moderate to dense chaparral vegetation. It was not very visible in the imagery used, only 35% being suggested by vintage stereo photographs, 13% in ADS40 Stereo and not at all in the LiDAR DEM.
- **Fault G** – This inferred fault trace is considerably reoriented, from a trace shown by California Division of Mines and Geology (1979), to correspond with several prominent lineations mapped across moderately to densely vegetated slopes.

Principally identified in vintage stereo photographs (71%), it was also detected in ADS40 Stereo (59%) and ADS40/NAIP fused with LiDAR DEM (57%). 45% of the trace was plotted on the LiDAR DEM shaded relief alone.

- **Fault H** – This inferred fault trace, from California Division of Mines and Geology (1979) is relocated to match some geomorphic features observed in this study. The feature lies within terrain covered by moderate to dense chaparral vegetation. 89% of the fault was seen in vintage stereo photographs and just less than half was seen in some LiDAR combinations. ADS40 Stereo and LiDAR DEM were each only able to detect 37% of this lineament. The expression of this lineament is principally larger-scale sidehill benches and offset streams – features for which LiDAR offers no real advantage. It remains possible that this feature is related to landsliding rather than faulting, but this could not be resolved by this effort.

G. Analysis and Discussion

While the numbers in the tables provide some simplistic comparisons, they do not highlight whether the different image types were revealing more or less of the same traces or whether each had their own strengths, detecting fault segments not seen in other imagery. A more careful assessment of the results, considering area characteristics (geology, topography and vegetation) and looking at each mapped fault trace revealed some trends, but no overwhelmingly stark contrasts. Image types are ranked (based on percent of fault detected) for each fault segment in Tables 5a-d. For most areas true stereo imagery (photographic or digital) detected the most fault traces.

The character of the underlying geology does not appear to have a systematic impact that is detectable in this limited study.

General comments on utility of the processed/derived imagery

Vintage Stereo Photographs – Both study areas were evaluated in black and white aerial photography from two time periods. 1930 imagery (scale ~1:18,000) predated most human modification of the landscape but tended to have limited resolution, particularly in vegetated areas of low contrast. 1953/54 imagery (1:20,000) had better resolution but suffered from slightly smaller scale and greater modification of the natural ground surface. Stereo viewing greatly aided interpretation of fault-related geomorphic features and the ability to detect lineaments that might be a composite of geomorphic and tonal elements. Lack of ortho-rectification or geographic registration presented accuracy issues in transferring the data to a modern digital base. The earliest photos, in particular, presented a problem where there were no cultural features to aid image registration and even vegetation patterns had changed. Due to the scale of the aerial photography, relative to some of the digital imagery, there was a tendency to interpolate continuous lineaments between closely spaced features. This may have biased the assessment of how completely a fault was mapped.

Indio study area

Fault Trace	TERRAIN / FIELD Conditions				Imagery Type							Best Imagery
	Slope	Vegetation	Geology	Remarks	AP	LiDAR	NAIP	STEREO	Draped	Fused		
									NAIP	NAIP T	NAIP F	
SAF-nw	low to moderate	light to moderate	Qp/Qal	multiple traces that are close together	4	4	4	3	5	5	5	STEREO with AP, LiDAR, NAIP
SAF-c	low to moderate	light	Qp/Qal		2	3	3	2	3	4	4	AP or STEREO
SAF-se	low	light	Qal	modified landscape	1		5	4	5	5	5	AP
SAF-NB(r)	low to mod to steep	light	Qo, Qp		4	5		4	5	4		AP, f-NAIP with STEREO
SAF-nw-a	low to moderate	low to moderate	Qo, Qp	parallel traces, oases	3	4	5	1	5	5	5	STEREO
SAF-Hope(r)	low to moderate	light to moderate	Qp	truncated old fans, oases			4					Field
NB-a	low	sparse	Qal, Qp	contrasting lithology	2		1	1	1	2	2	Color Imagery (NAIP, d-NAIP or STEREO)

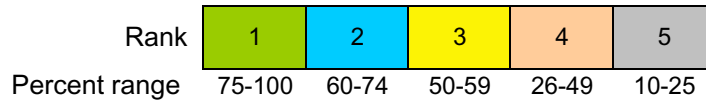


Table 5a. Imagery types with rankings of value for mapping each fault trace.

Yucaipa study area

NW Block

Fault Trace	TERRAIN / FIELD Conditions				Imagery Type									BEST IMAGERY	
	Slope	Vegetation	Geology	Remarks	AP	LiDAR	NAIP	ISTAR	STEREO	Draped		Fused			
										NAIP	ISTAR	NAIP T	NAIP F		
SAF-1w	moderate to high	moderate to dense	gg/Qof,Qyf	separates geologic units	5	4					5	5			LIDAR
SAF-1ww	moderate	moderate	gg/Qof,Qyf	faceted slopes	1	4			3	3			4		AP
SAF-1we	moderate	light to moderate	gg	alignment of features	1	1	4		1	3			5		AP or Stereo, LiDAR
SAF-2w	moderate to low	light to moderate	Qof,Qyf		4	4			4	4	4	4	4	4	all together
Fault-Aw	moderate to high	moderate	gg,Qyf	offset streams, ridges	2	3	4		3	4			5		AP with STEREO, LiDAR
Fault B	high to moderate	light to moderate	gg		4	2	4	5	3	2	4				LiDAR
Fault C	moderate to high	light to mod to dense	gg	hillslope features	3	3						4			AP or LiDAR
Fault I	moderate	light to medium dense	Qof,Qyf	man-made structures	1	4						5		5	AP

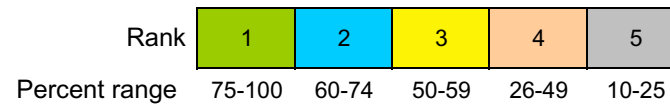


Table 5b. Imagery types with rankings of value for mapping each fault trace.

Yucaipa study area

SE Block

Fault Trace	TERRAIN / FIELD Conditions				Imagery Type									BEST IMAGERY
	Slope	Vegetation	Geology	Remarks	AP	LiDAR	NAIP	ISTAR	STEREO	Draped		Fused		
										NAIP	ISTAR	NAIP T	NAIP F	
SAF-1e	moderate to high	moderate to dense	landslide	sag pond	1	2	5		2	4		4	4	AP STEREO/LiDAR
API-1se	moderate to high	moderate to dense	landslide		3	1			3	5		3	4	LiDAR
SAF-2e	high to moderate	moderate to dense	landslide		4	4	4		4	4		4	4	LiDAR, AP or f-NAIP
Fault-F	moderate to high	moderate to dense	landslide		4				5				5	AP
Fault-G	moderate	moderate to dense	Qoal		2	4	4		3	5	5	3	4	AP
SAF-H	moderate	moderate to dense	landslide	sidehill bench	1	4	4		4	4	4	4	4	AP



Table 5d. Imagery types with rankings of value for mapping each fault trace.

LiDAR DEM Shaded Relief – LiDAR DEM shaded relief was derived from the filtered (minimum elevation value) data to present at least two illumination directions – orthogonal to the fault from the northeast and from the southwest with low angles of 20 to 30 degrees. Illumination orthogonal to the general fault trend was found to be useful for detecting fault-parallel geomorphic features. Many features were more easily seen under an alternative lighting angle, and so it was beneficial to switch regularly between the two illumination directions. It was also critical to interpret the imagery at several different scales, down to the resolution of the imagery (~1:1000). The clarity of the geomorphic surface, as well as ARCGIS tools to analyze surfaces, facilitated the refinement of fault locations identified in LiDAR or other imagery.

Some lineaments, evident in vintage stereo photographs, were not observed in the LiDAR images, perhaps due to the lack of color or tone in the images. The LiDAR DEM shaded relief was obviously of limited value in modified terrain. In the Yucaipa area it was noted that observable features were less sharp than in the Indio area, perhaps due to the reduced ground returns through the vegetation. Ultimately, it was found useful to use the lineaments from the vintage stereo photographs to focus attention on some of the more subtle features that might otherwise have been missed.

Several artifacts in the imagery presented false lineaments that needed to be identified and rejected. These occurred primarily at the edges of overlapping swaths. At some locations, the surface texture, including typical corduroy effect, were truncated at the artifacts and were readily flagged (Figure 7a). However, there were some very convincing artifacts in the Indio study area that required a field check to be certain that they were not real (Figure 7b).

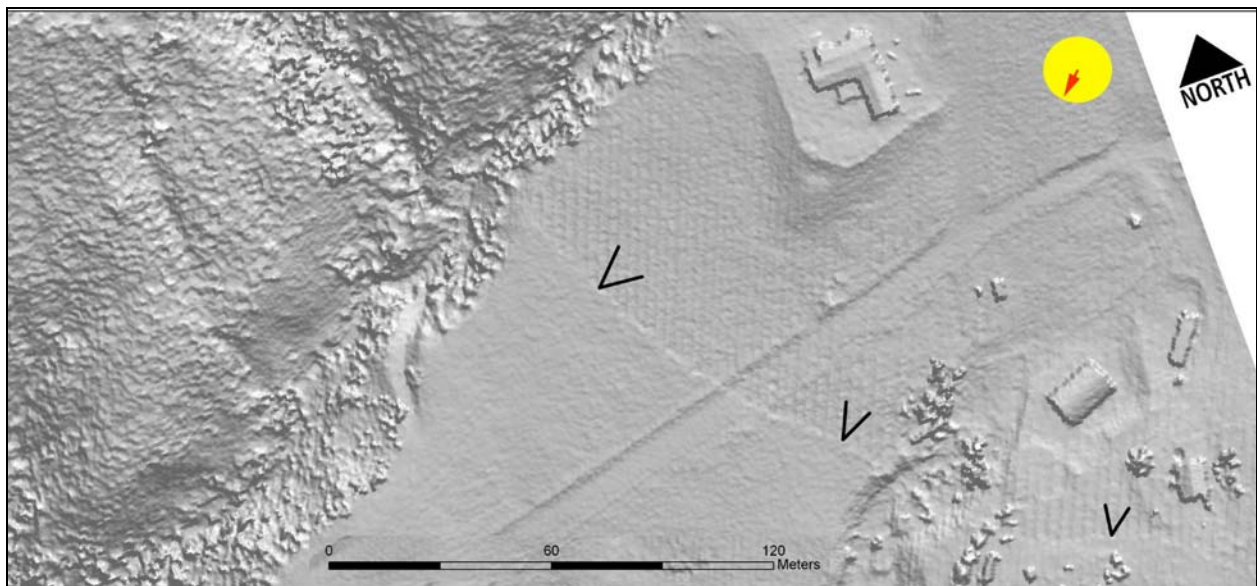


Figure 7a. LiDAR artifact (arrows) in the Yucaipa study area. The artifact appears as a linear highlight suggestive of an east-facing scarp. However, the evident “corduroy” texture on one side versus the other alerts one to the likelihood that this is an artifact. Indeed, it corresponds to the overlap margin between LiDAR swaths.

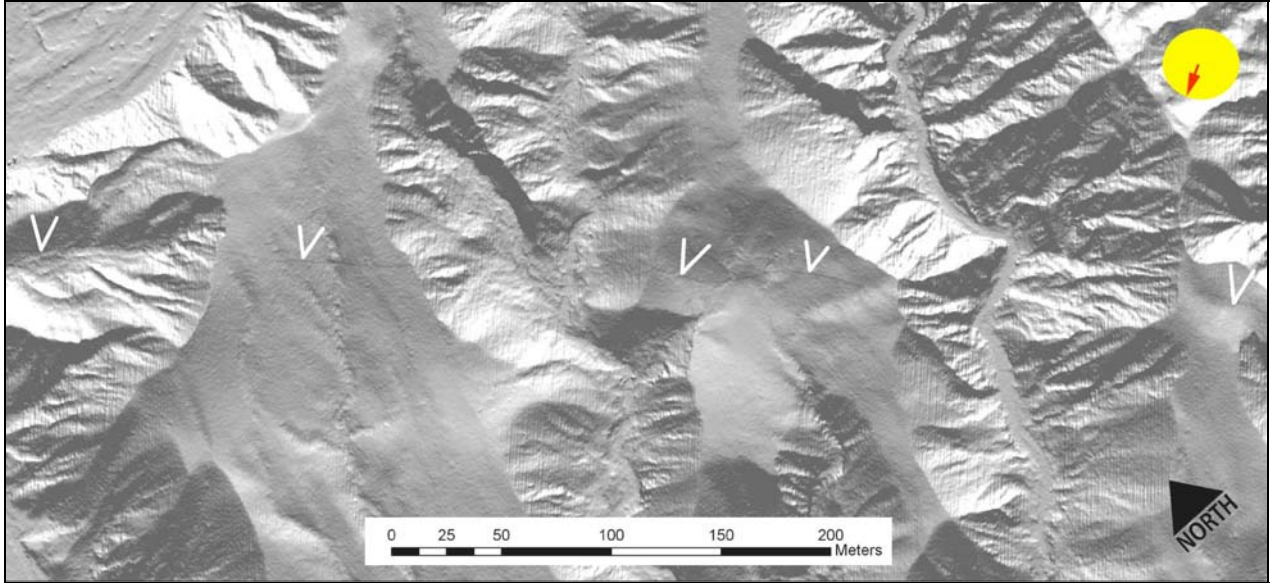


Figure 7b. This LiDAR artifact (arrows) in the Indio study area was more tempting to believe. It parallels the known fault trends and appeared to be a consistent low southwest-facing scarp. Even more deceptive was its prominence on older surfaces, where an old scarp might be expected, and its absence in most of the intervening eroded areas. Field inspection found no evidence of the feature, and reference to a plot of the LiDAR shot density showed that it coincided with a swath overlap margin.

-- (Both LiDAR DEMs are illuminated from the northeast)

ADS40/NAIP – This flat imagery was a challenge to use and interpret, and it was often difficult to differentiate real tonal contrasts from shadows. Relief was difficult to interpret, with many topographic features being essentially invisible. The imagery was especially limited in vegetated terrain. It performed relatively better in the sparsely vegetated Indio study area, comparing favorably with the LiDAR for the main trace of the San Andreas Fault. Some limited interpretation was attempted on one false-color rendering but no advantage was seen in this exercise. A related study (Perez and others, 2008) may find more utility to some multi-spectral, hyper-spectral and thermal imagery combinations.

ADS40/ISTAR – The utility of this imagery as compared with ADS40/NAIP was even more limited, with many of the same difficulties. Only a few vegetation lineaments or contrasts were noted, several of these resulting from riparian vegetation. Features that were noted were just as likely to be unrelated to faulting as they were to be along faults. One notable exception was in the Mill Creek floodplain where several possibly significant lineaments were only observed in the ISTAR image and its derivatives. (One vegetation lineament was also seen in the 1930 photography, a resource that is not always available). The ISTAR imagery was only available for the Yucaipa study area.

ADS40 Stereo – The digital stereo imagery was superior to other imagery in many areas, particularly in areas of sparse vegetation and moderate relief. It was almost

universally at least equal to the combined imagery (draped or fused) for mapping faults. The addition of true stereo viewing to the high resolution and digital accuracy of these images provided excellent results. Different degrees of vertical exaggeration could be achieved by using different look angle combinations in the stereo pairs. The ability to adjust brightness and contrast facilitated fault identification in some areas. It was simple, and useful for analysis, for more than one interpreter to view the stereo model at the same time, limited only by the number of stereo glasses available. As expected, the ADS40 Stereo was somewhat less useful than LiDAR in the more heavily vegetated slopes of the Yucaipa area.

ASTER VNIR – Due to the low resolution of the ASTER imagery it was only useful at the scale needed for this study to highlight some very crude lineaments. When lineaments were mappable, it was difficult to interpret a cause for the lineament without comparison to other imagery where they were readily visible. Due to the coarseness of the imagery the locational accuracy was also very poor. One unintended consequence of the crude imagery was that the eye tends to interpolate more and fill in gaps with the result that the ASTER imagery yielded a misleading degree of completeness in identifying some traces. For these same reasons it was blind to additional parallel fault traces.

COMBINATION IMAGERY

Draped over LiDAR DEM shaded relief -

- *ADS40/NAIP* – Interpretation was done at multiple scales and alternate illumination directions and, as with the LiDAR alone, these techniques increased the number of features that could be interpreted. It was anticipated that the addition of true color to the detailed LiDAR DEM shaded relief would be a benefit, however, the ADS40/NAIP overlay appeared to mask many details that were seen in the LiDAR alone – an effect that was mitigated to some extent by toggling the ADS40/NAIP image off. The benefit of identifying cultural and vegetation features from the addition of color was slight in these particular study areas.
- *ADS40/ISTAR* – As the primary difference between the ISTAR imagery and the true-color ADS40/NAIP imagery is the addition of the IR spectrum, the interpretation was focused on vegetation patterns, without noting some features that were merely visible from the underlying LiDAR DEM. As with the ISTAR alone, just as many non-fault features were observed as were fault-associated features. An additional step was taken to see if the draped image helped extend or connect features already identified in other imagery but such enhancement was not seen, except perhaps as already seen with ISTAR alone on the Mill Creek floodplain.
- *ASTER VNIR* – This combination appeared to add very little, if anything, to the interpretation of the LiDAR alone and results were not compiled.

Fused with LiDAR DEM - (resulting combination imagery inherits the higher resolution of the LiDAR DEM)

- ADS40/NAIP (true color) – This combination appeared to be most useful in the Yucaipa area, especially in the southeastern block and somewhat less on the Mill Creek floodplain. Largely it enabled mapping of features already mapped from other single image types or combinations, although the unique fusing of color and topography did highlight one subtle fault extension on the older fan surface of Mill Creek (API-2). Little benefit was seen in the Indio area except for highlighting one interior fault (SAF-NBr) that was mostly also detected by the ADS40 Stereo image. The inability to toggle the ADS40/NAIP contribution, as was done in the draped image, was sometimes a hindrance to interpretation.
- ADS40/NAIP (false color) – Results for this false color combination were very similar to the true color fused image, and it appeared to add some features not seen in the true color fused image. Bedrock structure, such as bedding, seemed to be somewhat more visible. However, this fused imagery did not appear to detect any fault features not seen in at least one of the single image types.
- ADS40/ISTAR – Interpretation was done at multiple scales. At smaller scales (~1:5500) this combination mainly highlighted aspect-related vegetation. At larger scales (1:2000 and larger) there was little benefit seen to this fused imagery and some features were less prominent than with the draped image pair.
- ASTER VNIR – no value was seen to this combination; only a few lineaments were plotted and they bore only weak correlation to features established from other sources. Results were not compiled.

Caveats or Limitations

Several factors should be mentioned, that may bear on the effectiveness of this study and also on the ability to apply these findings to other situations. First, the hoped-for thoroughness of the analysis was hindered by difficulties with the hardware and software for digital stereo viewing and interpretation. As a result, the ADS40 stereo interpretation was performed by different team members than those who interpreted the other imagery. There was a general comparability in the experience and ability of the interpreters, but any differences could not be quantified within the constraints of this project. Another variable was the consistency with which we were able to interpret features from one image set to the next, due to increasing familiarity with the terrain and/or interpreter fatigue. Ideally an iterative process might be used to make the evaluation more uniform.

Additionally, judgments as to the accuracy of fault location from any particular imagery set were compromised to some degree by the inability to a) define a precise location from subdued or subtle features and b) to define a precise location for the actual fault with which we compared our results. Poor exposures in many parts of the field area, particularly the Yucaipa area, also restricted our ability to verify and locate the faults. The actual faults may also be longer or shorter than shown, affecting the reported proportion of the fault that was seen. Some identified features may not be faults (e.g. fault NB-a in the Indio area) and some actual faults probably would not have been detected if we weren't looking for them (e.g. SAF-Hope(r) in the Indio area or Faults Ac or SAF-1c in the Yucaipa area).

Accuracy and Precision

The accuracy as well as resolution of the georeferenced digital data allowed us to use it as the standard for location of many identified fault features. The LiDAR data, with the highest resolution and greatest surface definition, was well suited to combine with other similarly well-located digital imagery. This is considered a great improvement over the classical interpretation of aerial photography alone.

One of the goals of this project was to assess improvements in the accuracy of plotting faults as identified in various image sets. This aspect did not get as rigorous a look as originally intended. Part of the reason is the inherent precision of the LiDAR and ADS40 Stereo platforms. What became readily apparent was that the precision of these data sets far exceeded the accuracy of the interpretation. Except for a few rare instances of fairly sharp fault scarps, most fault expression was such that a fault location could not be interpreted with an accuracy of greater than perhaps two to five meters, and as much as 10 meters variance in vegetated or eroded terrain with more subdued features. This is considerably larger than the 0.5 m pixel resolution of the LiDAR and the 0.76 to 0.87 m pixel resolution of the ADS40 imagery. Hence, we did not have an accurate enough reference, in the case of inferred and approximately located faults, to judge the accuracy of interpretation from these digital image sources.

However, we did succeed, in an early phase of this project, in improving the locational accuracy of features interpreted in unregistered vintage aerial photographs (1930 and 1953/54). We were able to make a first approximation, within a GIS platform, for the location of various interpreted features by warping and stretching the images to a close approximation of the USGS topographic map for the area. We then overlaid the 1930 and 1953/54 data layers on a LiDAR-derived DEM shaded relief base. It became apparent in many instances that 1) features from different images that plotted in somewhat different locations were in fact the same feature, and 2) that these features could be relocated to match the same feature visible in the LiDAR DEM shaded relief. In this way we were able to significantly improve the accuracy of these fault feature locations. Even non-geomorphic features could be relocated. This was done in two ways. Clusters of features, both tonal and geomorphic, could be warped and shifted as a group based on the geomorphic features alone. Also, tonal and vegetation lineaments could be corrected to match the ADS40 imagery. We do not have a quantitative assessment of this improvement, but some examples may be seen in Figure 8.

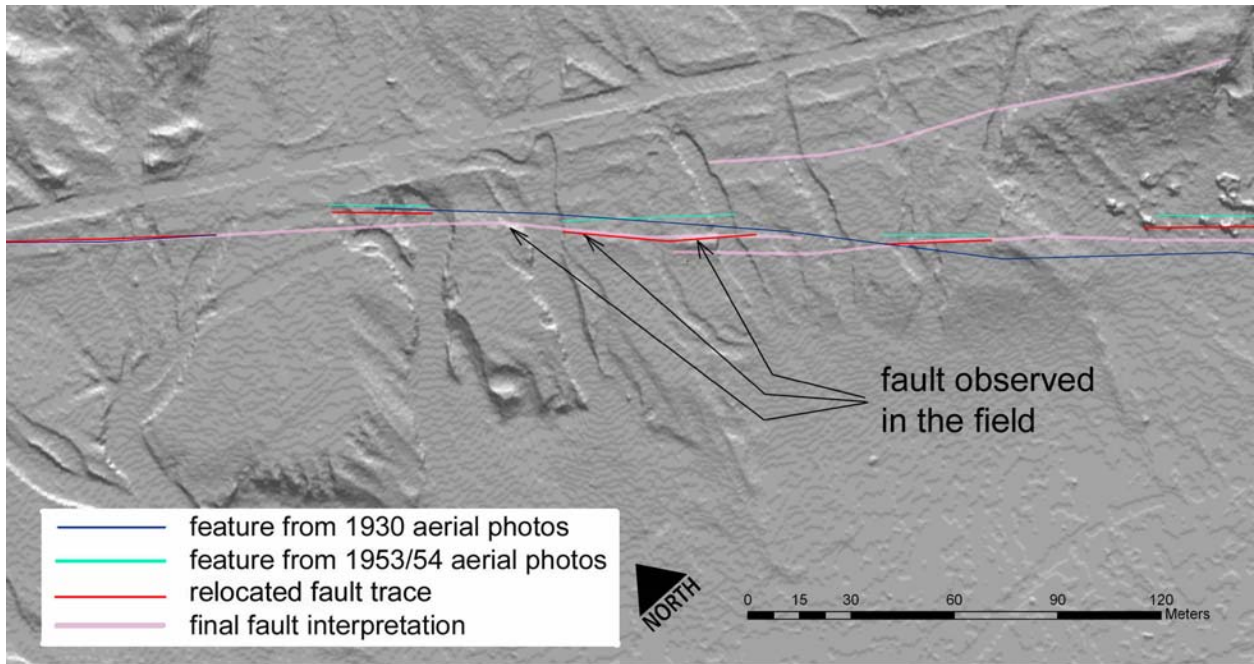


Figure 8a. Similar lineaments were plotted from both the 1930 and the 1953/54 aerial photos in the Indio area, but in slightly different locations approximately 1-10 meters apart. Each of these were up to 5 meters from probably correlative features in the LiDAR DEM shaded relief. Field mapping corroborated several of the relocated features. (*LiDAR DEM illuminated from the northeast*).

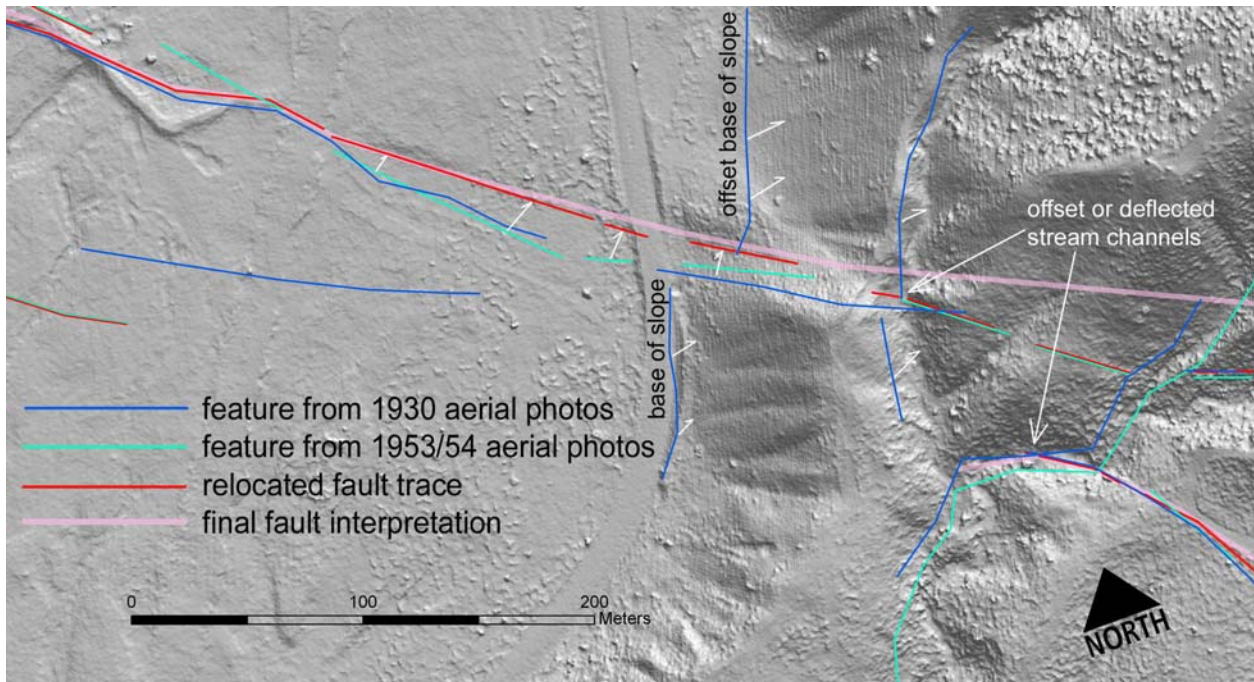


Figure 8b. A well-expressed fault in the Mill Creek floodplain could be readily identified in the LiDAR DEM shaded relief, allowing relocation of a scarp plotted from aerial photography. The error was as much as 20 meters. Other offset geomorphic features could also be accurately relocated. (*LiDAR DEM illuminated from the northeast*).

H. Conclusions

Although there are no overwhelming trends, this study demonstrated that true stereo (ADS40 Stereo and Vintage Stereo Photographs) was often the best imagery for identifying faults in terrain with any relief and the LiDAR DEM offered advantages in terrain with moderate to heavy vegetation. If you take away the clear advantage that vintage aerial photography has in areas that were subsequently modified, ADS40 Stereo seemed to be the superior platform for observing faults in areas of light vegetation. This advantage over vintage aerial photography is probably a result of the higher resolution of the digital imagery, with some additional benefit due to variable vertical exaggeration and adjustable brightness and contrast. In areas of heavier vegetation, LiDAR and vintage aerial photography were the stronger media.

There were always exceptions and most other imagery or combinations certainly added fault elements not seen in the three principal platforms. However, these exceptions were often not clearly attributable to conditions of vegetation, relief or geology, although the ability to see vegetation lineaments (ISTAR and NAIP) proved advantageous in otherwise low-relief areas. Digital imagery (LiDAR or ADS40) with high resolution (1 m pixel or less) provides the best accuracy for fault location and is very useful for improving fault locations from either published mapping or aerial photo interpretation. Image types other than LiDAR had an advantage of sensing tonal differences, which very often help define, connect, extend or reinforce geomorphic lineaments. The low-resolution of the ASTER data, even when fused with the LiDAR DEM shaded relief, seriously hampered its usefulness to a mapping effort at the scale made possible by the other imagery.

Ultimately, we believe that it was the use of multiple image types that allowed greater completeness of fault trace mapping in the areas studied, with an increase in accuracy of location dependent on digital imagery. Repeated observation of a trace in multiple image types provided reinforcement for fault interpretation. Even small fault elements, uniquely identified in one image type, in aggregate with other imagery provided necessary continuity to lineament interpretation. Draped or fused imagery added value for some faults, but the additional processing involved in the fusion process may not be justified by the minimal improvements seen in this study. The identification of some strong lineaments that probably are not fault related also reinforced the need for ground truth in any geologic studies.

LiDAR data is freely available, but only along specific narrow swaths where data have already been collected (www.opentopography.org). This is fine for well-defined and well-understood faults but can be frustrating where unanticipated splay faults and local complications extend beyond the LiDAR coverage. ADS40 Stereo imagery currently exists for the entire state of California; wider availability is being explored. The results of this study show that investment in making this data more readily available and usable will have significant benefits for many mapping interests, including fault mapping.

I. Resultant Publications

- Treiman, J.A and Perez, F.G., 2009, Utility of combined aerial photography and digital imagery for fault trace mapping: (abstract) Southern California Earthquake Center, Annual Meeting, Palm Springs, September 2009
- Perez, F.G., Treiman, J.A, and Bryant, W.A., 2010, Utility of combined aerial photography and digital imagery for fault trace mapping: (abstract and poster presentation) American Society for Photogrammetry and Remote Sensing Annual Conference, San Diego, CA, April 2010.

J. Further work

- Perez, F., Treiman, J., and Bryant, W., 2008, Use of Integrated Master Multispectral Imagery and LiDAR DEM for Active Fault Detection and Evaluation: NASA proposal, funded for 2009-2010.

K. Acknowledgements

We wish to acknowledge the assistance of our colleagues at the California Geological Survey: Tim McCrink for his invaluable assistance in working with the ADS40 stereo imagery in stereo analyst and in imagery slicing, Carlos Gutierrez for ArcGIS database management and troubleshooting, Chuck Real, Tim McCrink and Chris Wills for advice, support and critical review of the manuscript.

Sincere thanks are due to the Open Topography team led by Chris Crosby (SDSC, Geoscience Coordinator & OpenTopography lead, GEON Project) who provided assistance and guidance in the acquisition of LiDAR imagery.

We are indebted to Jonathan Matti, at the US Geological Survey, who made the 1930 Spence aerial photos available for our use in the Yucaipa area. We also benefited from the knowledge he shared about the geology and structure of the area and the encouragement to pursue our own findings.

L. References

- Bevis, M., Hudnut, K., Sanchez, R., Toth, C., Grejner-Brzezinska, D., Kendrick, E., Caccamise, D., Raleigh, D., Zhou, H., Shan, S., Shindle, W., Yong, A., Harvey, J., Borsa, A. Ayoub, F., Shrestha, R., Carter, B., Sartori, M., Phillips, D., and Coloma, F., 2005, The B4 Project: scanning the San Andreas and San Jacinto fault zones: American Geophysical Union, Fall Meeting Abstracts, abstract #H34B-01
- Bonkowski, M.S., 1981, Tectonics, geomorphology and neotectonics of the San Andreas fault zone, Indio Hills, Coachella Valley, California: unpublished M.A. thesis, U.C. Santa Barbara. [map not available]
- California Division of Mines and Geology, 1974, Official Map, Special Studies Zones, SW ¼ Lost Horse Mtn. Quadrangle: California Division of Mines and Geology, 1:24,000.
- California Division of Mines and Geology, 1979, Revised Official Map, Special Studies Zones, Yucaipa Quadrangle: California Division of Mines and Geology, 1:24,000.
- Clark, M.M., 1984, Map showing recently active breaks along the San Andreas Fault and associated faults between Salton Sea and Whitewater River-Mission Creek,

- California: U.S. Geological Survey, Miscellaneous Investigation Series Map I-1483, 1:24,000.
- Hope, R.A., 1969, Recently active breaks along the San Andreas and related faults between Cajon Pass and the Salton Sea: U.S. Geological Survey Open-File Report OFR 69-130, 1:24,000
- Keller, E. A., Bonkowski M.S., Korsch R.J., and Shlemon, R.J., 1982, Tectonic geomorphology of the San Andreas fault zone in the southern Indio Hills, Coachella Valley, California: Geological Society of America Bulletin, v.93, p. 46-56.
- Matti, J.C., Morton, D.M., Cox, B.F., Carson, S.E., and Yetter, T.J., 2003, Geologic map and digital database of the Yucaipa 7.5' quadrangle, San Bernardino and Riverside Counties, California: U.S. Geological Survey Open File Report 03-301, version 1.0.
- McCrink, T. P., Perez, F. G., and Yoha, R. E., 2006, Evaluation of NAIP/ADS40 stereo imagery for GIS-based landslide inventory mapping at the California Geological Survey, CGS Tech. Doc. 2006-2, p.30.
- McCrink, T. P., and Perez, F. G., 2006, Instruction manual for slicing and exporting NAIP stereo imagery from the 2005 California National Agricultural Imagery Project for use in Stereo Analyst for ArcGIS, CGS Tech. Doc. 2010-1, p.2.
- Perez, F., Treiman, J., and Bryant, W., 2008, Use of Integrated Master Multispectral Imagery and LiDAR DEM for Active Fault Detection and Evaluation: NASA proposal, funded for 2009-2010.
- Popenoe, F.W., 1959, Geology of the southeastern portion of the Indio Hills, Riverside County, California: unpublished M.A. thesis, U.C.L.A, 153p., map 1:31,250
- Prentice, C.S., Koehler, R.D. III, Baldwin, J.N., Harding, D.J., 2004, Evaluation of LiDAR Imagery as a tool for mapping the northern San Andreas Fault in heavily forested areas of Mendocino and Sonoma Counties, California [abs.]: EOS, Transactions of the American Geophysical Union, v. 85(47), Fall Meeting Supplement, Abstract G11B-07.
- Whitehill, C.S., Prentice, C.S., and Mynatt, I., 2009, LiDAR-based mapping of the northern San Andreas and Hayward Faults, California (abstract): Seismological Research Letters, v.80, no.2, p.304.

M. Appendices

Table 3a. Fault-related geomorphic features mapped in the Indio study area.

Table 3b. Fault-related geomorphic features mapped in the Yucaipa study area.

Table 3a. FAULT-RELATED GEOMORPHIC FEATURES MAPPED IN THE INDIO STUDY AREA

ID	Geomorphic Feature	KEY: ld - linear drainage vc - vegetation contrast lr - linear ridge dd - deflected drainage tl - tonal lineament vl - vegetation lineament bd - beheaded drainage cd - closed depression lt - linear trough sp - sag pond tc - tonal contrast s - saddle pa - ponded alluvium sc - scarp dr - deflected ridge dsc - deflected stream channel shb - sidehill bench bis - break in slope			Source (f - fused with LiDAR DEM) (d - draped over LiDAR shaded relief)	VISIBLE (y=yes, n=no, p-partial)							Photo re-check (nv-not visible)
						Comments	Field Notes	Aerial Photo	LiDAR	ADS40/NAIP T	ADS40 Stereo	ASTER	
1	drainage		aligns with lineament to the SE	f-NAIP T	n	n			n	n	y	n	
2	lineament (sharp)		tl; perhaps bedding	f-NAIP T	n	n			n	n	y	n	
3	drainage			LiDAR	y	n			n	n	n	n	
4	channel margin			LiDAR	y	n			n	n	n	n	
5	scarp (weak)			f-NAIP T	n	n			n	n	y	n	
6	scarp (weak)		v.weak; more of a hint of feature	LiDAR	y	n			n	n	n	n	
7	scarp (weak)		very low but abrupt	LiDAR	y	n			n	n	n	n	
8	scarp (distinct)		very low but abrupt	LiDAR	y	n			n	n	n	n	
11	scarp (distinct)		v.low but abrupt	LiDAR	y	n			n	y	n	n	nv
12	scarp (distinct)		abrupt	LiDAR	y	n			n	y	p	y	nv
13	scarp (weak)		base of linear ridgelet	d-NAIP	n	y			n	y	n	n	
14	scarp (distinct)		v.low but abrupt	LiDAR	y	n			n	y	y	y	nv
16	scarp (weak)		greatly reduced scarp?	d-NAIP	y	n			n	y	n	n	
17	lineament (sharp)		tl	f-NAIP F	n	n			n	n	n	y	
18	scarp (distinct)		not very distinct [photo 5496-5497]	f-NAIP T	n	n			n	p?	y	y	
19	scarp (distinct)		anomalous gully	f-NAIP T	y	y			n	y?	y	y	
20	lineament (sharp)		tc	f-NAIP T	n	n			n	n	y	n	
21	lineament (weak)		tl	f-NAIP T	n	n			n	n	y	n	
22	lineament (weak)		tc	f-NAIP T	n	n			n	n	y	n	
23	scarp (weak)		margin of saddle behind gentle anticline	LiDAR	y	n	p		n	p	n	n	
24	drainage			LiDAR	y	n	n		n	n	n	n	
25	drainage			LiDAR	y	n	n		n	n	n	n	
26	scarp (distinct)			LiDAR	y	n	n		n	y	n	n	
27	drainage			LiDAR	y	n	n		n	n	n	n	
28	drainage		linear drainage	d-NAIP	y	n	y		n	y	n	n	
29	lineament (sharp)		poss. vl	LiDAR	n	y	n		n	n	n	n	
30	lineament (weak)		poss.vl	LiDAR	n	y	n		n	n	n	n	
31	scarp (weak)			LiDAR	n	y	n		n	n	n	n	
32	lineament (weak)		tl; poss. sw-facing scarp?	f-NAIP T	n	y	n		n	n	y	n	
33	scarp (distinct)		may be trail (or trail may follow feature?); extends further SE than plotted	LiDAR	n	y	n		n	n	n	n	
34	scarp (weak)		abrupt backfacing scarp; saddle aligns with >35<	f-NAIP T	n	n	n	y	n	y	y	n	
35	scarp (weak)		saddle [photo 5521, 5522]	f-NAIP T	n	n	n	y	n	y	y	n	
36	scarp (weak)		back edge of terrace [photo 5521, 5522]	f-NAIP T	n	n	n	y	n	n	y	n	
37	scarp (weak)		?	f-NAIP T	y	n	n	n	n	y	y	n	
38	drainage			f-NAIP T	y	n	n		n	y	y	n	
39	scarp (distinct)		abrupt backfacing scarp [photo 5518, 5523, 5524]; old Qt to NE matches Qt above >285<; extends further SE than plotted	LiDAR	n	y	n		n	n	y	n	
40	scarp (weak)			LiDAR	n	y	n		n	n	n	n	
41	drainage		swales flanked by gravel bars; possible bar/swale on older surface or ridge spread	LiDAR	n	y	n		n	n	n	n	
42	drainage		swales flanked by gravel bars; possible bar/swale on older surface or ridge spread	LiDAR	n	y	n		n	n	n	n	
43	drainage		not likely to be fault associated [p1524]	d-NAIP	n	n	n		n	y	n	n	
44	scarp (weak)		truncated small ridges	NAIP	n	n	y		n	n	n	n	
45	lineament (weak)		vl	NAIP	n	n	y		n	n	n	n	
46	lineament (weak)		vl	NAIP	n	n	y		n	n	n	n	
47	lineament (sharp)		vl	d-NAIP	n	n	n		n	y	n	n	
48	lineament (weak)			d-NAIP	n	n	n		n	y	n	n	
49	lineament (weak)		vl	NAIP	n	n	y		n	n	n	n	
50	scarp (weak)		in shadow	LiDAR	n	y	n	n	n	n	n	n	
51	lineament (weak)		mole track or vl	LiDAR	n	y	n	n	n	n	n	n	
52	scarp (distinct)		excellent scarp offsets old fan surface ~2m vertical & ~7m r.l. [5538 ff]	LiDAR	y	y	n	y	n	y	y	y	
53	scarp (distinct)		or sharp ridge	d-NAIP	n	n	n	y	n	y	n	n	
54	lineament (weak)		tonal contrast	LiDAR	y	y	n	y	n	n	n	n	
55	scarp (distinct)		possibly fluvial	LiDAR	n	y	p	n	n	n	y	y	
56	lineament (weak)		tonal contrast	LiDAR	y	y	n	y	n	n	n	n	
57	scarp (weak)		appears to be road cut	LiDAR	n	y	y	n	n	n	y	y	
58	scarp (weak)		verified	LiDAR	y	y	y	y	n	n	y	y	
59	drainage			LiDAR	n	y	n	n	n	n	n	n	
60	scarp (weak)		not well-defined	LiDAR	y	y	y	y?	n	n	y	y	
61	channel margin		probably fluvial	LiDAR	n?	y	n	n	n	n	n	n	
62	lineament (weak)		tl	d-NAIP	n	n	n	p	n	y	n	n	
63	scarp (distinct)		poss. bedding control	LiDAR	n	y	n	y	n	n	n	n	
64	scarp (weak)			LiDAR	y	y	n	n	n	n	n	n	
65	scarp (distinct)			LiDAR	y	y	n	p	n	y	y	y	
66	lineament (sharp)		tonal contrast	LiDAR	y	y	n	y	n	n	y	y	
67	scarp (weak)		backside of linear ridge?	LiDAR	n	y	n	n	n	n	n	n	
68	lineament (weak)		tonal lineament	LiDAR	n	y	n	n	n	n	n	n	
69	lineament (weak)		saddle/offset ridge, right	LiDAR	n	y	n	n	n	n	n	n	
70	scarp (distinct)			LiDAR	n	y	n	?	n	n	n	n	
71	scarp (distinct)			LiDAR	n	y	n	?	n	n	n	n	
72	faceted spur		verified	LiDAR	n	y	n	n	n	n	n	n	
73	lineament (weak)		base of slope?	LiDAR	y	y	y	y	n	y	y	n	
74	lineament (weak)		tonal lineament	LiDAR	y	y	y	y	n	y	y	y	
75	lineament (weak)		tonal contrast	LiDAR	y?	y	y	p	n	n	y	n	
76	faceted spur		poor, diffuse	LiDAR	n	y	n	n	n	n	n	n	
77	scarp (weak)		tl	NAIP	n	n	y	p	n	y	n	n	
78	lineament (sharp)		vl or tc	NAIP	?	n	y	y	n	n	n	n	
79	scarp (weak)		possibly artificial	f-NAIP F	y?	y	n	n	n	n	y	y	
80	channel margin		right offset channel margin	LiDAR	n	y	n	n	n	n	n	n	
81	channel margin		right offset channel	LiDAR	n	y	n	n	n	n	n	n	
82	channel margin		offset drainage, right	LiDAR	n	y	n	n	n	n	n	n	
83	channel margin		offset drainage, right	LiDAR	n	y	n	n	n	?	n	n	
84	scarp (distinct)		nothing sharp noticeable; anomalous gravel bar below may be offset fan; prob. mislocated note for 365	LiDAR	n	y	n	n	n	n	y	y	

Table 3a. FAULT-RELATED GEOMORPHIC FEATURES MAPPED IN THE INDIO STUDY AREA

ID	Geomorphic Feature	KEY:		Source (f - fused with LiDAR DEM) (d - draped over LiDAR shaded relief)	VISIBLE (y=yes, n=no, p-partial)							Photo re-check (nv-not visible)	
		Comments	Field Notes		Aerial Photo	LIDAR	ADS40/NAIP T	ADS40 Stereo	ASTER	Draped ADS40/NAIP	Fused ADS40/NAIP T		Fused ADS40/NAIP F
85	scarp (distinct)	poss. fluvial enhanced	not visible; no fluvial enhancement	LiDAR	n	y	n	n	n	n	n	n	
86	channel margin		very young erosional feature	LiDAR	n	y	n	n	n	n	n	n	
87	channel margin		very young erosional feature	LiDAR	n	y	n	n	n	n	n	n	
88	channel margin	part of channel set parallel to s	very young erosional feature	LiDAR	n	y	n	n	n	n	n	n	
89	lineament (weak)	poss. wk. SW-facing scarp	very young erosional feature	LiDAR	n	y	n	n	n	n	n	n	
90	lineament (weak)	tonal contrast	possible scarp with trail along base	LiDAR	n	y	n	n	n	n	n	n	
91	lineament (sharp)	base of slope?/tonal contrast	verified 9/16; bench at base suggests second close parallel strand	LiDAR	y	y	n	n	n	n	y	y	
92	faceted spur		verified 9/16	LiDAR	?	y	n	n	n	n	n	n	
93	drainage	right offset at front	verified 9/16	LiDAR	n	y	y	n	n	y	n	n	
94	channel margin	poss. multiple offsets	too many meanders to judge significance	LiDAR	n	y	y	n	n	y	n	n	
95	channel margin	poss. multiple offsets	too many meanders to judge significance	LiDAR	n	y	n	n	n	n	n	n	
96	lineament (weak)	tonal contrast		LiDAR	n	y	n	n	n	n	n	n	
97	lineament (weak)	tonal lineament		LiDAR	n	y	n	n	n	n	n	n	
98	lineament (weak)	v. weak on surfaces, not in young channels; possible road		LiDAR	n	y	n	n	n	n	n	n	
99	lineament (weak)	poss. rt. offset stream		LiDAR	n	y	n	n	n	n	n	n	
100	lineament (weak)	poss. rt. offset stream		LiDAR	n	y	n	n	n	n	n	n	
101	channel margin	beheaded/reoccupied drainage	superceded by >103<	LiDAR	p	y	n	n	n	y	n	n	
102	channel margin	left-lateral? - deflection?		LiDAR	n	y	?	n	n	n	n	n	
103	channel margin	beheaded drainage	[p5526] superceded by next parallel channel to the east >104<	LiDAR	p	y	n	n	n	p	n	n	
104	channel margin	offset drainage, right	[p5527]	LiDAR	n	y	n	n	n	y	n	n	
105	channel margin			LiDAR	n	y	n	n	n	y	n	n	
106	scarp (weak)	aligned with offset drainage		LiDAR	n	y	n	n	n	n	n	n	
107	channel margin	possible scarp	erosional scarp	LiDAR	n	y	n	n	n	n	n	n	
108	scarp (weak)			LiDAR	n	y	n	n	n	n	n	n	
109	scarp (weak)		not believable	LiDAR	n	y	n	n	n	n	y	n	
110	lineament (weak)			LiDAR	n	y	n	n	n	n	y	n	
111	scarp (weak)	difficult to locate		f-NAIP T	y	?	y	y	n	n	y	y	
112	lineament (weak)	vl	part verified	NAIP	n	n	y	p	n	n	n	n	
113	lineament (weak)	tc	not evident on surface	d-NAIP	n	n	n	n	n	y	n	n	
114	lineament (sharp)	tl		NAIP	n	n	y	n	n	n	n	n	
115	lineament (sharp)	poss. S-facing low scarp	not visible; bedding appears continuous	d-NAIP	n	n	n		n	y	n	n	
116	lineament (weak)	tl	not evident in arroyo margin	f-NAIP T	n	n	n		n	n	y	n	
117	drainage		no fault visible	f-NAIP T	n	n	n		n	n	y	n	
118	drainage			f-NAIP T	n	n	n		n	n	y	n	
119	scarp (weak)		vertical shear zone in west arroyo bank [1514-17]	f-NAIP T	n	n	n		n	n	y	n	
120	scarp (weak)		shears not visible on this side of arroyo	f-NAIP T	n	n	n		n	n	y	n	
121	scarp (weak)			f-NAIP T	n	n	n		n	n	y	n	
122	scarp (distinct)	v.low but abrupt	artifact of LiDAR scan edge; not present in field	LiDAR	n	y	n		n	n	y	y	nv
123	drainage			LiDAR	n	y	n		n	n	y	n	
124	scarp (distinct)		not visible	LiDAR	n	y	n		n	n	n	n	
125	scarp (weak)		not visible	LiDAR	?	y	n		n	n	n	n	
126	lineament (weak)	vl	probably controlled by bedding	NAIP	n	n	y		n	n	n	n	
127	lineament (weak)	tc	clay beds	NAIP	n	n	y		n	n	n	y	
128	scarp (weak)		small degraded scarp ~1m high & 30° at steepest	LiDAR	n	y	n		n	n	n	n	
129	scarp (weak)	poss. abandoned channel margin	margin of gravel deposit	LiDAR	n	y	n		n	n	n	n	
130	scarp (distinct)		rock cairn on western part of trace	NAIP	n	n	y		y	y	n	n	
131	scarp (weak)		with >134< appears to be erosional remant of vertical gravel bed [photo 5528-5529]	LiDAR	n	y	n		y	y	n	n	
132	scarp (weak)		possible fault [p5528-29]	LiDAR	n	y	n		n	y	y	n	
133	scarp (weak)			LiDAR	n	y	n		n	y	y	n	
134	scarp (weak)		see >131< [p5528-29]	f-NAIP F	?	n	n		n	n	y	y	
135	scarp (distinct)		helps define SW side of linear ridge	LiDAR	y	y	n	n	y	n	y	y	
136	faceted spur			LiDAR	n	y	n	y	n	n	n	n	
137	scarp (distinct)		helps define SW side of linear ridge	LiDAR	y	y	y	?	y	n	y	y	
138	faceted spur			LiDAR	n	y	n	?	n	n	n	n	
139	scarp (distinct)			LiDAR	n	y	n	y	?	n	n	n	
140	faceted spur			LiDAR	n	y	n	n	n	n	n	n	
141	scarp (weak)			LiDAR	n	y	y	y	?	n	n	n	
142	channel margin		~5m r.l.	LiDAR	n	y	n	y	n	n	n	n	
143	channel margin		see >142<	LiDAR	n	y	n	y	n	n	n	n	
144	scarp (weak)		drainage deflection aligns with backside of linear ridge; rock cairn on trace	d-NAIP	n	n	n	y	n	y	n	n	
145	drainage			d-NAIP	n	n	n		n	y	n	n	
146	scarp (distinct)	poss.dissected	parallel bench/ridge/bench at SE end; perhaps two close strands	LiDAR	n	y	y		n	n	y	y	
147	lineament (sharp)	base of slope		LiDAR	n	y	n	n	n	n	y	n	
148	scarp (weak)		abundant efflorescence; vegetation above scarp	LiDAR	?	y	y	y	n	y	n	n	
149	channel margin			d-NAIP	n	n	n		n	y	n	n	
150	channel margin	right offset		d-NAIP	n	n	n	n	n	y	n	n	
151	scarp (weak)	or veg contrast and erosional bank		f-NAIP T	n	n	n	n	n	n	y	n	
152	scarp (weak)		verified	LiDAR	?	y	n	y	?	n	n	n	
153	channel margin		road cut	LiDAR	n	y	n	n	n	n	n	n	
154	channel margin			LiDAR	n	y	n	n	n	y	n	n	
155	scarp (weak)		saddle, deflected steams, ridges & thin vegetation line [photo 5530]	d-NAIP	n	n	n	n	n	y	n	n	
156	lineament (weak)	vl	not visible	d-NAIP	n	n	n	n	n	y	n	n	
157	channel margin	upper channel bank		LiDAR	n	y	n	n	n	n	n	n	
158	channel margin	lower channel margin		LiDAR	n	y	n	n	n	n	n	n	
159	lineament (weak)	aligned vague features	linear bench deflects/disrupts small SW-flowing drainages; 4-5 m r.l.	LiDAR	y	y	n	n	n	n	n	n	
160	lineament (weak)	vl	deflects small drainage (r.l.) at NW end	d-NAIP	n	n	n	n	n	y	n	n	
161	scarp (weak)			LiDAR	n	y	n	n	n	n	n	y	
162	lineament (weak)	tonal contrast; poss. base of slope	at base of slope; minor 1m right-lateral offset of small gullies; possibly not real	LiDAR	n	y	p	n	n	y	y	y	
163	lineament (sharp)	tl	band of carbonate (?) visible on ground may have created SE part of lineament	NAIP	y	n	y	y	n	n	n	n	
164	scarp (distinct)			NAIP	y	n	y	y	n	n	n	n	
165	scarp (weak)			LiDAR	y	y	n	y	n	n	n	y	
166	scarp (weak)			d-NAIP	n	n	n	n	n	y	n	n	
167	scarp (weak)			LiDAR	y	y	y	y	n	n	n	y	
168	lineament (weak)	line of saddles?	beheads several drainages; bench margin	LiDAR	n	y	y	y	n	y	n	n	
169	scarp (weak)		beheads /offsets small drainage WPT014, 015	LiDAR	n	y	n	n	n	n	y	n	
170	scarp (weak)			LiDAR	n	y	y	y	?	y	y	n	

Table 3a. FAULT-RELATED GEOMORPHIC FEATURES MAPPED IN THE INDIO STUDY AREA

ID	Geomorphic Feature	Comments	Field Notes	Source (f - fused with LiDAR DEM) (d - draped over LiDAR shaded relief)	VISIBLE (y=yes, n=no, p-partial)							Photo re-check (nv-not visible)	
					Aerial Photo	LIDAR	ADS40/NAIP T	ADS40 Stereo	ASTER	Draped ADS40/NAIP	Fused ADS40/NAIP T		Fused ADS40/NAIP F
171	scarp (weak)		verified; irregular base of scarp	f-NAIP F	?	n	y	y	n	n	n	y	
172	scarp (weak)			f-NAIP T	n	n	n	n	n	n	y	n	
173	scarp (weak)		defines SW side of possible shutter ridge	f-NAIP F	n	n	n	y	n	y	y	y	
174	scarp (weak)		upstream of WPT016; possible shutter ridge and offset upstream [p5534]	LiDAR	n	y	?	n	n	y	n	n	
175	scarp (weak)		sidehill bench [photo 5536]	LiDAR	n	y	n	y	y	n	n	n	
176	scarp (weak)			LiDAR	n	y	n	y	y	n	n	n	
177	lineament (weak)	vague tonal lineament		LiDAR	n	y	n	n	y	n	n	n	
178	scarp (weak)		WPT016; possible shutter ridge and offset upstream [p5532-33]	LiDAR	y	y	p	p	n	n	y	y	
179	scarp (weak)			LiDAR	n	y	n	n	n	n	n	n	
180	scarp (weak)		irregular base of slope	f-NAIP F	n	n	?	n	n	n	y	y	
181	lineament (weak)	tl or NE-facing scarp		f-NAIP F	n	n	n	n	n	n	y	y	
182	scarp (weak)	unusual shadow lineament		LiDAR	n	y	n	n	n	n	n	n	
183	scarp (weak)			LiDAR	n	y	n	n	n	n	n	n	
184	scarp (weak)	unusual shadow lineament not on upper surf.		LiDAR	n	y	n	n	n	n	n	n	
185	scarp (weak)			f-NAIP T	n	n	n		n	n	y	n	
186	lineament (sharp)	drainage and saddle		f-NAIP F	n	n	n		n	n	n	y	
187	lineament (sharp)	saddle		f-NAIP F	n	n	n		n	n	n	y	
188	scarp (weak)			f-NAIP T	n	n	n		n	n	y	y	
189	scarp (distinct)			f-NAIP F	n	n	n		n	n	y	y	
190	scarp (distinct)			LiDAR	n	y	n		n	n	y	n	
191	scarp (weak)			f-NAIP T	n	n	n		n	n	y	n	
192	lineament (weak)	disconnect of topo features; rl offset of ridge?		f-NAIP F	n	n	n		n	n	p	y	
193	scarp (weak)			LiDAR	n	y	n		n	n	n	n	
194	scarp (weak)			LiDAR	n	y	n		n	n	n	n	
195	scarp (distinct)			LiDAR	n	y	n		n	n	n	y	
196	scarp (weak)			LiDAR	n	y	n		n	n	n	y	
197	scarp (distinct)			f-NAIP F	n	n	n		n	n	n	y	
198	channel margin			f-NAIP F	n	n	n		n	n	n	y	
199	scarp (distinct)	poss. artifact?		f-NAIP F	n	y	n		n	n	n	y	
200	scarp (weak)		parallel to bedding	LiDAR	n	y	n		n	n	n	n	
201	scarp (distinct)	possible abandoned channel margin	parallel to bedding	LiDAR	n	y	n		n	n	n	n	
202	lineament (sharp)	tl		f-NAIP T	n	n	n		n	n	y	n	
203	scarp (distinct)			LiDAR	n	y	n		n	n	y	y	
204	scarp (distinct)			LiDAR	n	y	n		n	n	n	y	
205	scarp (weak)			LiDAR	n	y	n		n	n	y	y	
206	scarp (weak)		parallel to bedding [photo 5466]	f-NAIP T	n	n	y		n	n	y	y	
207	scarp (distinct)		parallel to bedding	f-NAIP T	n	n	y		n	n	y	y	
208	scarp (distinct)			f-NAIP T	n	n	y		n	n	y	y	
209	lineament (sharp)	probably bedding	oblique to bedding [photo 5465]	NAIP	n	n	y		n	n	n	?	
210	lineament (sharp)	vl and drainage		NAIP	n	n	y		n	n	n	n	
211	scarp (weak)		linear drainage margin; cuts across bedding	f-NAIP T	n	n	n		n	n	y	n	
212	lineament (sharp)	vl or bedding	linear drainage margin; probable right-lateral offset drainage [photo 5464]	NAIP	n	n	y		n	n	n	n	
213	scarp (weak)	poss. backside of shutter ridge		LiDAR	y	y	n	y	y	n	n	n	
214	scarp (weak)			LiDAR	n	y	p	n	n	n	n	n	
215	scarp (weak)			f-NAIP T	n	n	n	p	n	n	y	y	
216	lineament (sharp)	tc		f-NAIP T	y	n	?	?	n	n	y	n	
217	lineament (weak)	poss. veg. lineament		LiDAR	n	y	n	?	n	n	n	n	
218	lineament (weak)	poss. veg. lineament		LiDAR	n	y	n	y	y	n	n	n	
219	lineament (sharp)	vc		d-NAIP	y	n	y	n	n	y	n	n	
220	channel margin		modified at both ends	LiDAR	n	y	n	n	n	n	n	n	
221	channel margin		see >220<	LiDAR	n	y	n	n	n	n	n	n	
222	scarp (weak)		irregular/modified?; not impressive	LiDAR	n	y	y	y	y	y	y	y	
223	lineament (weak)	tc		f-NAIP T	y	n	y	y	y	y	y	y	
224	lineament (weak)	tc		f-NAIP T	y	?	y	y	y	y	y	y	
225	lineament (weak)	tc/tl		f-NAIP T	y	y	y	y	y	y	y	y	
226	scarp (weak)	and vl		NAIP	p	n	y		n	n	n	n	
227	lineament (sharp)	vl	parallel to bedding [photos 5467 & 5468 show possible fault@WPT002]	d-NAIP	y	n	y	y	y	y	n	p	
228	lineament (sharp)	vegetation lineament	drainage along bedding; [photo 5466]	NAIP	p	n	y	y	y	y	?	y	
230	lineament (sharp)	vc		d-NAIP	p	n	y	y	n	y	n	y	
231	lineament (weak)	vc		d-NAIP	n	n	y	y	n	y	?	y	
232	lineament (sharp)	vc		d-NAIP	p	n	y	y	n	y	?	y	
233	lineament (weak)	vl		NAIP	n	n	y	y	n	n	n	n	
234	lineament (sharp)	vl		d-NAIP	n	n	n	n	n	y	n	n	
235	lineament (sharp)	tc		f-NAIP T	n	n	n	n	n	n	y	n	
236	lineament (sharp)	tc	WPT006; probable groundwater difference; otherwise difficult to ascribe cause; shallow bedrock	NAIP	n	n	y	y	y	n	n	n	
237	scarp (distinct)	poss. artificial	may be road cut	f-NAIP F	n	n	n	n	n	n	n	y	
238	scarp (distinct)			f-NAIP F	n	n	y	n	n	y	n	y	
239	scarp (weak)		no scarp, but is boundary between dissected/undissected terrain	LiDAR	n	y	n	n	n	y	n	n	
240	scarp (weak)	{probably related to bedding}	vertical bedding and/or shears in expansive f.g. silt is just SW of channel margin	f-NAIP F	n	y	y	n	n	y	n	y	
241	channel margin			f-NAIP F	n	n	y	n	n	n	n	y	
242	scarp (weak)		probably erosional	f-NAIP F	n	n	n	n	n	n	n	y	
243	scarp (weak)			LiDAR	n	y	n	n	?	n	n	n	
244	scarp (weak)		linear ridge with slightly uneven base of slope on NE side	f-NAIP F	y	y	p	n	?	p	n	y	
245	scarp (weak)		linear ridge, SW side has one or two minor right-lateral offset swales	LiDAR	y	y	y	y	?	y	y	y	
246	scarp (distinct)		very linear front; offset drainages 1.5-2m r.l., WPT007-009 [photos 5481 & 5482 - stereo]	LiDAR	y	y	y	y	?	y	p	y	
247	lineament (weak)	vc	WPT010 at SE projection; small anticline N. of main fault [photo 5483]	NAIP	?	n	y	n	?	n	n	n	
248	scarp (weak)			f-NAIP F	n	n	n	n	n	n	n	y	
249	lineament (sharp)	tc - poss. artificial		f-NAIP T	n	n	n	n	n	n	y	n	
250	scarp (distinct)	may be artificial		LiDAR	n	y	n	n	n	n	n	n	
251	scarp (distinct)			LiDAR	n	y	n	n	n	n	n	n	
252	scarp (weak)		scarp with rock cairn marking prior fracturing	LiDAR	n	y	n	n	n	n	n	y	
253	scarp (weak)		discontinuous scarp marked with rock cairn along prior fracturing; fault visible at NW end in stream cut	LiDAR	y	y	n	n	n	y	n	y	

Table 3a. FAULT-RELATED GEOMORPHIC FEATURES MAPPED IN THE INDIO STUDY AREA

ID	Geomorphic Feature	KEY: ld - linear drainage dd - deflected drainage bd - beheaded drainage sp - sag pond pa - ponded alluvium dsc - deflected stream channel	vc - vegetation contrast tl - tonal lineament cd - closed depression tc - tonal contrast sc - scarp shb - sidehill bench	lr - linear ridge vl - vegetation lineament lt - linear trough s - saddle dr - deflected ridge bis - break in slope	Source (f - fused with LiDAR DEM) (d - draped over LiDAR shaded relief)	VISIBLE (y=yes, n=no, p-partial)							Photo re-check (nv-not visible)	
						Aerial Photo	LIDAR	ADS40/NAIP T	ADS40 Stereo	ASTER	Draped ADS40/NAIP	Fused ADS40/NAIP T		Fused ADS40/NAIP F
		Comments	Field Notes											
254	scarp (distinct)				LiDAR	y	y	n	n	n	y	n	y	
255	scarp (weak)				LiDAR	y	y	n	n	n	?	n	n	
256	channel margin	offset in channel margins			LiDAR	n	y	n	n	n	n	n	n	
257	channel margin	offset channel margins			LiDAR	n	y	n	n	n	n	n	n	
258	channel margin				LiDAR	n	y	n	n	n	n	n	n	
259	channel margin				LiDAR	n	y	n	n	n	n	n	n	
260	channel margin				LiDAR	n	y	n	n	n	n	n	n	
261	scarp (weak)				LiDAR	n	y	n	n	n	n	n	n	
262	scarp (distinct)				LiDAR	n	y	n	y	n	n	n	n	
263	scarp (distinct)				LiDAR	n	y	n	y	n	n	n	n	
264	scarp (weak)				LiDAR	n	y	n	y	n	n	n	n	
265	channel margin				LiDAR	n	y	n	n	n	n	n	n	
266	channel margin				LiDAR	n	y	n	n	n	n	n	n	
267	channel margin				LiDAR	n	y	n	n	n	n	n	n	
268	channel margin				LiDAR	n	y	n	n	n	n	n	n	
269	channel margin				LiDAR	n	y	n	n	n	n	n	n	
270	lineament (weak)	tc			NAIP	y	n	y	n	n	y	n	n	
271	channel margin				LiDAR	n	y	n	n	n	n	n	n	
272	channel margin				LiDAR	n	y	n	n	n	n	n	n	
273	lineament (weak)	vegetation contrast; base of slope			LiDAR	y	y	y	y	y	y	y	y	
274	lineament (weak)	vegetation?			LiDAR	n	y	n	n	n	n	n	n	
275	drainage	poss. road			LiDAR	n	y	n	n	n	n	n	n	
276	lineament (weak)	tc			f-NAIP T	y	n	y	y	y	y	y	y	
277	lineament (sharp)	vc			f-NAIP T	y	y	y	y	y	y	y	y	
278	lineament (weak)	ill-defined tc/vc			f-NAIP F	n	n	n	n	n	n	n	y	
279	lineament (weak)				wbAst_Geo	?	n	n	p?	y	n	n	n	
280	lineament (weak)	tc			f-NAIP T	n	n	n	n	n	n	y	n	
281	lineament (weak)				wbAst_Geo	n	n	n		y	y	n	n	
282	scarp (distinct)	possibly man-made			LiDAR	n	y	n	n	n	n	n	n	
283	scarp (distinct)	with 282, possibly man-made			LiDAR	n	y	n	n	n	n	n	n	
284	scarp (weak)	r.l. offset ridge at NW end			LiDAR / Field	n	y	n		n	n	n	n	
285	scarp (distinct)	bank of linear trough			LiDAR / Field	n	n	n	n	n	n	n	n	
286	channel margin	opposite bank of linear trough			LiDAR / Field	n	n	n	n	n	n	n	n	
287	lineament (weak)				field 5/12/09	n	n	n	n	n	n	n	n	
288	scarp (distinct)				field 5/12/09	n	n	n	y	n	n	n	n	
289	ridgeline				field 5/12/09	n	n	n	n	n	n	n	n	
290	scarp (weak)				field 5/12/09	n	n	n	n	n	n	n	n	
291	vl	vl			Stereo				y					
292	s	s			Stereo				y					
293	vl	vl			Stereo				y					
294	sc-e, dd-r	sc-e, dd-r			Stereo				y					
295	sc-w, tc	sc-w, tc			Stereo				y					
296	vl	vl			Stereo				y					
297	tl, lt	tl, lt			Stereo				y					
298	tc	tc			Stereo				y					
299	sc-e	sc-e			Stereo				y					
300	tl, shb	tl, shb			Stereo				y					
301	sc-w, dd-l	sc-w, dd-l			Stereo				y					
302	s, ddr	s, ddr			Stereo				y					
303	dr, sc-w	dr, sc-w			Stereo				y					
304	s, vl	s, vl			Stereo				y					
305	sc-w, vl	sc-w, vl			Stereo				y					
306	sc-e	sc-e			Stereo				y					
307	vc	vc			Stereo				y					
308	sc-e, ddr	sc-e, dsc-r			Stereo				y					
309	tl	tl			Stereo				y					
310	sc-e	sc-e			Stereo				y					
311	sc-w, vc	sc-w, vc			Stereo				y					
312	sc-w, vc	sc-w, vc			Stereo				y					
313	vc	vc			Stereo				y					
314	sc-w, tl	sc-w, tl			Stereo				y					
315	tl, sc-w, s	tl, sc-w, s			Stereo				y					
316	ddr, sr	dd-r, sr			Stereo		y	y	y		y			
317	sc-w	sc-w			Stereo				y					
318	ddr	dd-r			Stereo			y	y		y			
319	shb	shb			Stereo				y					
320	ddr	dd-r			Stereo				y		y			
321	lr	lr			Stereo				y					
322					Stereo				y					
323					Stereo				y					
324					Stereo				y					
325					Stereo				y					
326	tl	tl			Stereo				y					
327					Stereo				y					
328					Stereo				y					
329					Stereo				y					
330					Stereo				y					
331					Stereo				y					
332					Stereo				y					
333					Stereo				y					
334					Stereo				y					
335	ddr	dd-r			Stereo				y					
336	sc-w	sc-w			Stereo				y					

Table 3a. FAULT-RELATED GEOMORPHIC FEATURES MAPPED IN THE INDIO STUDY AREA

ID	Geomorphic Feature	Comments	Field Notes	Source (f - fused with LiDAR DEM) (d - draped over LiDAR shaded relief)	VISIBLE (y=yes, n=no, p-partial)								Photo re-check (nv-not visible)
					Aerial Photo	LIDAR	ADS40/NAIP T	ADS40 Stereo	ASTER	Draped ADS40/NAIP	Fused ADS40/NAIP T	Fused ADS40/NAIP F	
337	vc	vc		Stereo				y					
338	sc-w	sc-w		Stereo				y					
339	vc	vc		Stereo				y					
340	vc	vc		Stereo				y					
341	vc	vc		Stereo				y					
342	sc-e, vc	sc-e, vc	back-facing slope parallels scarp to NE; possible graben	Stereo				y					
343	sc-e, vc	sc-e, vc	back-facing slope parallels scarp to NE; possible graben	Stereo				y					
344	vc, sc-e	vc, sc-e	back-facing slope parallels scarp to NE; possible graben	Stereo				y					
345	vc	vc		Stereo				y					
346	sr, lr, vc	sr, lr, vc	partial shutter ridge below palms; sidehill bench at palms may be on bedding	Stereo				y					
347	vc, ddr	vc, dsc-r	no faults evident in intermittent exposures in stream bank	Stereo	y			y					
348	ddr	dsc-r		Stereo	y			y		y			
349	vc	vc		Stereo	y			y		y			
350	vl	vl	steep scarp	Stereo				y					
351	sc-w	sc-w	steep scarp, poss. man-made; 35-degree slope [p5462]	Stereo				y					
352	sc-w	sc-w	follows edge of road; WPT010 at NW end - small anticline N. of main fault [photo 5483]	Stereo				y					
353	sc-w, vl	sc-w, vl		Stereo				y					
354	sc-w	sc-w		Stereo				y					
355	vl	vl		Stereo	y			y					
356	tl	tl		Stereo	y			y					
357	tl	tl		Stereo	y			y					
358	lineament		beheads numerous small drainages; also includes saddles at SW end (168)	NAIP	y	n	y	n	n	n	n	n	n
359	lineament (weak)	saddles & shears	truncates alluvial surface to south; includes saddles, shear zones and align	Field 9/15/09									
360	lineament (sharp)	shear zone	shear zone in stream cut and across bedrock to the northwest	Field 9/15/09									
361	lineament (sharp)	shear/contrast; aligns w/305	prob. fault in stream bank separates clay on the N from pebbly clay to S [p5651]	Field 9/15/09									
362	lineament (sharp)	shear zone trends 160	fault zone in bluff trends through oasis; strikes 160 and near vertical [p5649-50]	Field 9/15/09									
363	channel margin	beheaded margin of old fan	margin of older fan is offset from SE of 70-72; intermediate fan lies SE of 363 in shadow of 72	Field 9/15/09									
364	lineament (sharp)	shear zone	shear zone in east side of wash trends 290-310; not visible in debris on west side [p1512-13]	Field 9/16/09									
365	faceted spur	possible old facet	weak feature lies within older offset fan remnant	Field 9/16/09									
366	faceted spur	small facet	small facet above trail	Field 9/16/09									
367	faceted spur		facet above trail	Field 9/16/09									
368	lineament (weak)	notch in ridgeline	flat bench/notch on ridgeline	Field 9/15/09									
369	drainage	right-deflected drainage	drainage deflected around 370 (shutter ridge?)	Field 9/15/09									
370	faceted spur	eroded; may be part of shutter	deflected drainage (369) behind	Field 9/16/09									
371	lineament (sharp)	notch/saddle w/shear; end of d	shear trend 312, 80NE; p5641	Field 9/15/09									
372	lineament (weak)	notch	observed in profile	Field 9/15/09									
373	drainage	right-deflected drainage	deflected behind possible shutter ridge [p5639-40]	Field 9/15/09									
374	faceted spur	very degraded	observed in field	Field 9/16/09									
375	lineament (sharp)	NE-dipping fault	north-dipping Palm Spring below flatter Ocotillo Fm. [p1470-73]; not a fault as originally thought from earlier visit	Field 9/16/09									
376	lineament (weak)	broad trough	broad bench or trough lies behind frontal fault zone; points towards canyon to NW	Field 9/16/09									
377	drainage	stops at bench	drainage stops at bench	Field 9/16/09									
378	drainage	approx.location deflected drain	pair of drainages with 4-5 m r.l. offset at bench	Field 9/16/09									
379	lineament (weak)	saddle separates gravel on SW	gravel cap on SW may be truncated by fault in saddle	Field 9/16/09									
380	lineament (weak)	saddle; offset ridge?; separates	probable continuation of 379	Field 9/16/09									
381	lineament (weak)	r.l. deflected drainages; efflores	probable continuation of 380	Field 9/16/09									
382	lineament (sharp)	offset drainage	offset drainage at palm; also observed in May'09 from 174	Field 9/16/09									
383	drainage	beheaded drainage	offset from 384	Field 9/16/09									
384	drainage	re-established drainage	drainage continues straight; old channel offset to 383	Field 9/16/09									
385	lineament (weak)	saddle above facet	part of aligned saddles with 386 and 373 and 316	Field 9/16/09									
386	lineament (weak)	saddle above facet (?)	aligned zone of weakness? behind 76 & 92; see 385	Field 9/16/09									
387	lineament (weak)	shallow trough; surface even ac	linear trough in old surface with no vertical offset apparent across feature	Field 9/16/09									
388	lineament (weak)	bench on slope	anomalous bench aligns with 387 [p1488-89]; also aligns with notch on trend 310	Field 9/16/09									
389	scarp (weak)	possibly modified by grading		LiDAR	y	y	n	n	n	n	n	n	n
399	scarp (weak)	vl; scarp in LiDAR profile		Stereo	y	n	n	y	?	n	n	n	n
400	scarp (weak)	vl; scarp in LiDAR profile		Stereo	y?	n	n	y	?	n	n	n	n
401	lineament (weak)	step in resistant lithology		Stereo	n	n	n	y	n	n	n	n	n
402	lineament (weak)	step in resistant lithology		Stereo	n	n	n	y	n	n	n	n	n
403	lineament (weak)	linear drainage & vegetation lineament		Stereo	y	p	n	y	n	n	n	n	n
404	lineament (weak)	vegetation lineament		Stereo	n	n	n	y	n	n	n	n	n
405	lineament (weak)	vegetation lineament		Stereo	n	n	n	y	n	n	n	n	n

Table 3b. FAULT-RELATED GEOMORPHIC FEATURES MAPPED IN THE YUCAIPA STUDY AREA

ID	Geomorphic Feature	KEY: ld - linear drainage vc - vegetation contrast lr - linear ridge dd - deflected drainage tl - tonal lineament vl - vegetation lineament bd - beheaded drainage cd - closed depression lt - linear trough sp - sag pond tc - tonal contrast s - saddle pa - ponded alluvium sc - scarp dr - deflected ridge dsc - deflected stream channel shb - sidehill bench bis - break in slope		Source (f - fused with LiDAR DEM) (d - draped over LiDAR DEM shaded relief)	VISIBLE (y=yes, n=no, p-partial)								photo re-check			
					Comments	Field Notes	Aerial Photo	LiDAR	ADS40/NAIP T	ADS40/ISTAR	ADS40 Stereo	Draped ADS40/NAIP		Draped ADS40/ISTAR	Fused ADS40/NAIP T	Fused ADS40/NAIP F
1	Scarp (distinct)			f-NAIP T	n	n	n	n		n	n	y	y	n	n	
2	Scarp (weak)			f-NAIP T	n	n	n	n		n	n	y	y	n	n	
3	Scarp (weak)	or linear drainage/base of slope		f-NAIP F	n	n	n	n		n	n	n	y	n	n	
4	Scarp (weak)			f-NAIP T	n	n	n	n		n	n	y	y	n	n	
5	drainage			ISTAR	n	n	n	y		y	n	n	n	n	n	
6	drainage			f-NAIP F	n	n	n	n		y	n	y	y	n	n	
7	Scarp (weak)			f-NAIP F	n	n	n	n		n	n	n	y	n	n	
8	ridgeline			f-NAIP F	n	n	n	n		n	n	n	y	n	n	
9	drainage			f-NAIP F	n	n	n	n		n	n	n	y	n	n	
10	Scarp (weak)			f-NAIP T	n	n	n	n		n	n	y	n	n	n	
11	Lineament (weak)	possible artifact?		f-NAIP F	n	n	n	n		n	n	n	y	n	n	
12	Scarp (weak)			f-NAIP T	n	n	n	n		n	n	y	n	n	n	
13	Scarp (weak)		weak	f-NAIP T	n	n	n	n		n	n	y	n	n	n	
14	Scarp (weak)		visible but eroded	LiDAR	n	y	n	n		n	n	p	n	n	n	
15	Scarp (weak)			LiDAR	p	y	n	n	n	n	n	y	n	n	n	
16	ridgeline			LiDAR	n	y	n	n		n	n	n	n	n	n	
17	drainage			d-NAIP	n	y	n	n		y	n	n	n	n	n	
18	Lineament (weak)	upper drainage & weak tl		d-NAIP	n	n	n	n		y	n	n	n	n	n	
19	Lineament (weak)	vl?		NAIP	n	n	y	n	n	n	n	n	n	n	n	
20	drainage			NAIP	n	n	y	n	n	n	n	n	n	n	n	
21	Scarp (distinct)		not visible in stream cut; good scarp and saddle at top	LiDAR	n	y	n	n	y	y	n	y	y	n	n	
22	Scarp (distinct)	vc	weak break-in-slope related to colluvial wedge at SE end; not visible at drainage to the NW	NAIP	n	n	y	n	p	n	n	n	n	n	n	
23	Scarp (weak)		not convincing	d-NAIP	n	n	n	n	n	y	n	n	n	n	n	
24	Lineament (weak)	weak drainage & saddle	scarplike at saddle, with probable ridge offset	d-NAIP	n	y	n	n	n	y	n	n	n	n	n	
26	faceted spur			f-NAIP F	n	n	n	n	n	n	n	n	y	n	n	
27	Scarp (weak)		principally a drainage margin	f-NAIP F	y	y	n	n	n	n	n	n	y	n	n	
28	Lineament (weak)	vl	not verifiable; perhaps a broad band of trees; lineament crosses saddle	NAIP	p	n	y	n	y	n	n	n	n	n	n	
29	ridgeline		may be edge of spur	LiDAR	n	y	n	n	n	n	n	n	n	n	n	
30	ridgeline		offset ridge from spur >31<	LiDAR	n	y	n	n	n	n	n	n	n	n	n	
31	faceted spur	dissected or imaginary	seems real and p of multiple parallel strands/saddles/facets	f-NAIP F	n	n	n	n	n	n	n	n	y	n	n	
32	Lineament (weak)	broad saddle	may be mislocated; saddle appears SW of plotted location	d-NAIP	n	n	n	n	y	y	n	n	n	n	n	
33	Lineament (weak)	ld	drainage margin - is actually rather irregular	LiDAR	n	y	n	n	y	y	n	n	n	n	n	
34	Scarp (weak)		steep side of small channel aligns with bench and saddle	LiDAR	n	y	n	n	p	y	n	n	n	n	n	
35	Lineament (sharp)			f-NAIP T	y	n	n	n	n	n	n	y	y	n	n	
36	Lineament (sharp)		not visible	f-NAIP T	p	n	n	n	n	n	n	y	y	n	n	
37	Lineament (weak)	vl	visible	NAIP	n	n	y	n	n	n	n	n	n	n	n	
38	drainage			LiDAR	y	y	n	n	n	y	n	n	n	n	n	
39	Scarp (weak)		most of feature to northwest is not visible	LiDAR	n	y	n	n	n	n	n	y	n	n	n	
40	Scarp (weak)	ambiguous highlight	margin of firebreak; may be fill artificially damming basin to SW	d-NAIP	n	n	n	n	n	y	n	n	n	n	n	?
41	Scarp (weak)	poss. modified?	firebreak	f-NAIP F	n	n	n	n	n	n	n	n	y	n	n	mod
42	ridgeline			d-NAIP	n	n	n	n	n	y	n	n	n	y	n	n
43	Scarp (weak)	edge of dissected bench	very prominent bench likely aligns with >46<	f-NAIP F	n	p	n	n	n	p	n	y	y	n	n	
44	Lineament (weak)	tl	questionable	d-NAIP	n	n	n	n	n	y	n	n	n	n	n	
45	Scarp (distinct)		edge of alluvial terrace	LiDAR	n	y	n	n	n	n	n	n	n	n	n	
46	Lineament (weak)	subtle bench	rather broad; may be 1n+/- m across	LiDAR	n	y	n	n	n	n	n	n	n	n	n	
47	Lineament (weak)	vl	can't verify	d-NAIP	n	n	n	n		y	n	n	n	n	n	
48	Scarp (weak)		distinct edge of basin or trough as it drops off to the southwest	f-NAIP T	n	n	n	n	n	n	n	y	y	n	n	
49	Scarp (weak)			LiDAR	n	y	n	n	n	n	n	n	n	n	n	
50	Scarp (weak)			LiDAR	n	y	n	n	n	n	n	n	y	n	n	
51	Scarp (weak)			LiDAR	n	y	n	n	n	n	n	n	y	n	n	
52	Lineament (sharp)	tl - cultural and/or edge of terrace		f-NAIP F	n	n	n	n	n	n	n	n	y	n	n	
53	Scarp (weak)			f-NAIP T	n	n	n	n		n	n	y	n	n	n	
54	drainage			d-NAIP	n	y	n	n		y	n	n	y	n	n	
55	drainage			d-NAIP	n	n	n	n		y	n	n	n	n	n	
56	Scarp (weak)			f-NAIP F	n	n	n	n		n	n	n	y	n	n	
57	Scarp (weak)			f-NAIP F	n	n	n	n		n	n	n	y	n	n	
58	Lineament (sharp)	vl (lack of veg)		ISTAR	n	n	n	y		n	n	n	n	n	n	
59	Lineament (sharp)	vl		ISTAR	n	n	n	y		n	n	n	n	n	n	
60	Scarp (distinct)		linear drainage on trend with saddles and facets to NW	LiDAR	y	y	n	n	y	n	n	n	n	n	n	
61	ridgeline	offset?		d-NAIP	n	n	n	n	n	y	n	n	n	n	n	
62	Scarp (weak)			f-NAIP F	n	n	n	n		n	y	n	y	n	n	
63	Lineament (weak)	saddle		d-NAIP	n	y	n	n	n	y	n	n	n	n	n	
64	Lineament (sharp)	vc		d-NAIP	n	y	y	y	n	y	y	n	n	n	n	
65	Scarp (weak)	break in slope	not visible; slope is loose grus near angle of repose; ledgy outcrop is upslope	d-NAIP	n	n	n	n	n	y	n	n	n	n	n	
66	Scarp (distinct)		erosional ridgelet down steep slope	LiDAR	?	y	n	n	n	n	n	n	n	n	n	
67	Lineament (weak)	vc; shrubs to south		d-ISTAR	n	y	n	n	n	n	y	n	n	n	n	
68	Scarp (weak)	or saddle		LiDAR	n	y	n	n	n	n	n	n	n	n	n	
69	Scarp (weak)		verified, with vegetation lineament to SE	LiDAR	n	y	n	n	n	n	n	n	n	n	n	
70	Scarp (weak)	low scarp	central p is prominent and appears to behead drainages; NW p not visible; possibly man-made	d-NAIP	n	n	n	n	n	y	n	n	n	n	n	old
71	Scarp (weak)	poss.subdued backfacing scarp		LiDAR	n	y	n	n	y	y	n	y	y	n	n	
72	Scarp (weak)		not verified -- dogs	LiDAR	n	y	n	n	?	y	y	n	n	n	n	
73	Scarp (distinct)	possibly erosional	not verified -- dogs	LiDAR	n	y	n	n	n	y	y	y	y	n	n	
74	Scarp (distinct)	possibly erosional	not verified -- dogs	LiDAR	y	y	n	n	n	n	y	y	y	n	n	
75	Lineament (weak)	comb.veg & tonal & scarp		d-ISTAR	n	n	n	n	n	n	y	n	n	n	n	
76	Lineament (weak)	tl		d-NAIP	n	n	n	n	n	y	n	n	n	n	n	
77	Lineament (sharp)	vc	not visible	f-NAIP F	n	n	n	n	n	n	n	n	y	n	n	
78	Scarp (weak)	subtle, dissected	exists above bench with oaks; equivocal cause [p5563]	LiDAR	n	y	n	n	n	n	n	n	n	n	n	
79	Scarp (distinct)	possibly man-made	check old photos for grading; very straight [p5562]; isolated/elevated surface south of lineament	f-NAIP T	y	y	n	n	y	n	n	y	y	n	n	nat
80	Scarp (distinct)	man-made?	possibly artificial - parallels powerline; linear bank and possibly deflected stream	f-NAIP T	y	y	n	n	n	y	y	y	y	n	n	
81	Scarp (distinct)	man-made?	road	f-NAIP T	y	n	n	n	y	n	y	y	n	n	n	
82	Scarp (weak)			f-NAIP F	n	n	n	n	n	n	n	n	y	n	n	
83	drainage			d-NAIP	n	n	n	n		y	n	n	n	n	n	
84	Lineament (sharp)	tl		d-NAIP	n	n	n	n		n	n	n	n	n	n	
85	Lineament (weak)	poss. resistant bdrk.		LiDAR	n	y	n	n		n	n	n	n	n	n	

Table 3b. FAULT-RELATED GEOMORPHIC FEATURES MAPPED IN THE YUCAIPA STUDY AREA

ID	Geomorphic Feature	KEY: ld - linear drainage dd - deflected drainage bd - beheaded drainage sp - sag pond pa - ponded alluvium dsc - deflected stream channel	vc - vegetation contrast tl - tonal lineament cd - closed depression tc - tonal contrast sc - scarp shb - sidehill bench	lr - linear ridge vl - vegetation lineament lt - linear trough s - saddle dr - deflected ridge bis - break in slope	Source (f - fused with LiDAR DEM) (d - draped over LiDAR DEM shaded relief)	VISIBLE (y=yes, n=no, p-partial)										photo re-check
						Aerial Photo	LiDAR	ADS40/NAIP T	ADS40/ISTAR	ADS40 Stereo	Draped ADS40/NAIP	Draped ADS40/ISTAR	Fused ADS40/NAIP T	Fused ADS40/NAIP F	Fused ASTER	
		Comments	Field Notes													
270	drainage				LiDAR	n	y	n	n	n	n	n	n	n	n	n
271	Lineament (sharp)	base of slope			LiDAR	y	y	n	n	n	y	n	n	n	n	n
272	Scarp (weak)	or vl?			f-NAIP F	y	n	n	n	n	n	n	y	n	n	n
273	drainage				d-NAIP	n	y	n	n	n	y	n	n	y	n	n
274	Lineament (sharp)	vc?	road area; uncertain significance; pipelines in area; poss. scarp below road; check aerials		f-NAIP F	y	n	n	n	y	n	n	n	y	n	n
275	Scarp (weak)				LiDAR	y	y	n	n	n	n	n	n	n	n	n
276	Scarp (weak)				d-NAIP	y	n	n	n	n	y	n	n	n	n	n
277	Scarp (weak)				d-NAIP	y	n	n	n	n	y	n	n	n	n	n
278	Scarp (weak)				LiDAR	y	y	n	n	y	n	n	n	n	n	n
279	Scarp (weak)	drainage margin			f-NAIP T	y	y	y	n	y	y	n	y	n	n	n
280	Scarp (distinct)				LiDAR	y	y	n	n	y	y	n	n	y	n	n
281	Scarp (distinct)	linear front			d-NAIP	n	n	n	n	n	y	n	n	n	n	n
282	Lineament (sharp)	vc			d-ISTAR	n	n	n	n	n	n	y	n	n	n	n
283	Lineament (weak)	diffuse saddle?	verified; with faceted slope above		d-NAIP	n	n	n	n	y	n	n	n	n	n	n
284	Lineament (weak)	strong but diffuse			d-ASTER	n	n	n	n	n	n	n	n	n	y	n
285	Lineament (sharp)	tl			d-NAIP	n	n	n	n	n	y	n	n	n	n	n
287	drainage		possible right-lateral offsets		Field/LiDAR	y	y	n	n	n	n	n	n	n	n	n
289	Lineament (sharp)		saddle behind offset ridge segment		Field 5/13/09	n	n	n	n	n	n	n	n	n	n	n
290	faceted spur		associated with >289<		Field 5/13/09	n	n	n	n	n	n	n	n	n	n	n
291	Lineament (weak)				f-NAIP T	n	n	n	n	n	y	n	y	n	n	n
292	Lineament (weak)				f-NAIP T	n	n	n	n	n	y	n	y	n	n	n
293	lt	lt	not visible		Stereo	y	n	n	n	y	n	n	n	n	n	n
294	tl	tl			Stereo	n	n	n	n	y	n	n	n	n	n	n
295	sc-e	sc-e	not verified; p road cut; enhanced by water tank cut at NW; looks more believable viewed from southeast		Stereo	y	n	n	n	y	n	n	n	n	n	n
296	vc,lt	vc,lt	not visible		Stereo	y	n	n	n	y	n	n	n	n	n	n
297	sc-w	sc-w			Stereo	y	n	n	n	y	n	n	n	n	n	n
298	sc-w	sc-w	probably man-made		Stereo	n	n	n	n	y	n	n	n	n	n	n
299	ddl	dd-l			Stereo	n	n	n	n	y	n	n	n	n	n	n
300	sc-w, s	sc-w, s	not noticeable; modified by cut		Stereo	y	n	n	n	y	n	n	n	n	n	n
301	vc, sc-w	vc, sc-w			Stereo	y	y	?	n	y	n	n	n	n	n	n
302	sc-w	sc-w	appears to coincide with margin of cut pad, probably man-made		Stereo	y	y	y	n	y	y	y	n	n	n	n
303	tl, dr, sc-w, vl	tl, dr, sc-w, vl	no scarp on slope; ply aligned with veg. contrast (poss. lithologic or structural control)		Stereo	y	n	n	n	y	n	n	n	n	n	n
304	vc	vc			Stereo	n	n	n	n	y	n	n	n	n	n	n
305	vc	vc			Stereo	n	n	n	n	y	n	n	n	n	n	n
306	vc	vc			Stereo	n	n	n	n	y	n	n	n	n	n	n
307	vc, ddr	vc, dsc-r			Stereo	y	n	n	n	y	n	n	n	n	n	n
308	vl	vl			Stereo	n	n	n	n	y	n	n	n	n	n	n
309	vl	vl			Stereo	n	n	n	n	y	n	n	n	n	n	n
310	tl	tl			Stereo	n	n	n	n	y	n	n	n	n	n	n
311	dr	dr			Stereo	n	n	n	n	y	n	n	n	n	n	n
312	vc	vc			Stereo	n	n	n	n	y	n	n	n	n	n	n
313	dr	dr			Stereo	n	n	n	n	y	n	n	n	n	n	n
314	vc	vc			Stereo	n	n	n	n	y	n	n	n	n	n	n
315	ld	ld			Stereo	y	y	n	n	y	y	n	y	y	n	n
316	lt	lt			Stereo	y	y	n	n	y	n	n	y	n	n	n
317	tl	tl	red soil to northeast of lineament		Stereo	n	n	n	n	y	n	n	n	n	n	n
318	ddr, ld	dd-r, ld			Stereo	y	y	n	n	y	n	n	n	n	n	n
319	sc-e	sc-e	seen; hard to differentiate from canyon margin		Stereo	n	n	n	n	y	y	n	n	n	n	n
320	ddr	ee-r			Stereo	y	y	n	n	y	n	n	n	y	n	n
321	sc-e	sc-e			Stereo	y	n	n	n	y	n	n	n	n	n	n
322	lt	lt	incised drainage with high bank or scarp on southwest		Stereo	n	y	y	n	y	n	n	n	n	n	n
323	s	s	visible		Stereo	y	n	n	n	y	n	n	n	n	n	n
324	sc-e, ld	sc-e, ld			Stereo	n	n	n	n	y	n	n	n	n	n	n
325	sc-e	sc-e	verified, with weaker matching rise to NE making shallow trough		Stereo	n	n	n	n	y	n	n	n	n	n	n
326	none	none	limited exposure inspected for faulting -- none observed		Field								y			
327	channel margin				d-NAIP		y	n	n	n	y	n	y	n	n	n
328	channel margin				d-NAIP		y	n	n	n	y	n	y	n	n	n
329	channel margin				d-NAIP		y	n	n	n	y	n	y	y	n	n
330	channel margin				d-NAIP		y	n	n	n	y	n	y	n	n	n